Exploiting Cell-Free Massive MIMO for Enabling Simultaneous Wireless Information and Power Transfer

Diluka Loku Galappaththige, *Student Member, IEEE*, Rajan Shrestha, and Gayan Amarasuriya Aruma Baduge, *Senior Member, IEEE*

arXiv:2010.13545v2 [eess.SP] 16 Nov 2020

***Abstract*—The performance of simultaneous wireless information and power transfer (SWIPT) in downlink (DL) cell-free massive multiple-input multiple-output (MIMO) is investigated. Tight approximations to the DL harvested energy and the DL/uplink (UL) achievable rates are derived for two practical channel state information (CSI) cases by using a non-linear energy harvesting model for time-switching and power-splitting protocols. Max-min fairness-based transmit power control policies are employed to mitigate the deleterious near-far effects caused by distributed transmissions/receptions in cell-free massive MIMO. The achievable common DL energy-rate trade-off is derived, and thereby, it is shown that the proposed max-min power control guarantees user-fairness regardless of near-far effects in terms of both harvested energy and achievable rate. The benefits of user estimated DL CSI to boost the SWIPT performance are explored. These performance metrics are compared against those of the conventional co-located massive MIMO, and thereby, it is revealed that the reduction of path-losses and lower average transmit powers offered by cell-free massive MIMO can be exploited to boost the energy-rate trade-off of SWIPT at the expense of increased backhaul requirements.**

***Index Terms*—SWIPT, Energy-rate trade-off, Distributed massive MIMO**

I. Introduction

The concept of wireless power transfer (WPT) was conceived by Nikola Tesla in the 1890s. It was originally intended for long-distance transmission of electrical energy from a power source to an electrical load without wired interconnections. Recently, the short-range WPT technology was rejuvenated for prolonging the battery-life of energy-constrained user nodes such as low-complexity sensors and Internet-of-Things (IoTs) [2]. In the downlink (DL) WPT, the energy is beamformed towards the users, and this harvest energy is typically stored or used to charge batteries. Then, a predefined fraction of the DL harvested energy can be used for uplink (UL) transmissions [3], [4].

By exploiting the broadcast nature of radio frequency (RF) wave propagation, the concept of simultaneous wireless information and power transfer (SWIPT) has been envisioned recently [5]–[7]. SWIPT techniques can be leveraged to prolong the battery-life or to serve as an alternative power source of energy-constrained, low-power wireless nodes in emerging IoTs [1], [5], [6], [8]–[12]. Deviating from separated information/energy receiver architectures [5], [7], two low-complexity co-located receiver structures, namely (i) the power-splitting (PS) receiver and (ii) the time-switching (TS) receiver, have been proposed in [6], [11] for enabling SWIPT in wireless systems. In PS receiver, the RF power captured by the rectenna is split based on a PS ratio by a power splitter and directed toward the information decoding and energy harvesting [6]. In TS receiver, the transmission duration is split into two orthogonal time-slots, which are then used for information and energy transmissions [6].

Despite its promise projected by early exploratory research with idealized system models [5], [6], the main inhibiting factors of enabling SWIPT in practical wireless networks include (i) inherent severe end-to-end path-loss [8], (ii) low radio frequency to direct current (RF-to-DC) conversion efficiency of rectennas [8], [9], and (iii) non-linear operating characteristics of energy harvesting circuitry [13]–[15]. Nonetheless, favorable propagation, channel hardening, and aggressive spatial multiplexing gains rendered by massive multiple-input multiple-output (MIMO) can be exploited to boost the performance gains of SWIPT [1], [8], [9].

Massive MIMO is originally conceived to serve many users in the same time-frequency resource element by exploiting aggressive spatial multiplexing gains offered by a very large co-located antenna array at a base-station (BS) [16]. Time-division duplexing (TDD) based co-located massive MIMO in sub-6 GHz frequency band has already been commercialized in the United States by Sprint [17], and it is one of the key enabling technologies of the fifth-generation (5G) standard [18]. Co-located massive MIMO is primarily intended for conventional cellular type deployments.

Recently, a cell-free massive MIMO architecture has been envisioned for wireless standards beyond 5G [19]. In cell-free massive MIMO, a large number of geographically distributed antennas or access-points (APs) simultaneously serves many users in the same time-frequency resource element in the TDD mode of operation. All APs are connected to a central processing unit (CPU) via a conventional backhaul network [20] or through a fronthaul network [21] where the CPU is a part of an emerging cloud-radio access network (C-RAN) [22]. The main difference between the cell-free massive MIMO and the well-established concepts of network MIMO [23], coordinated-multipoint (CoMP) [24], and distributed antenna systems (DAS) [25] is that the perspectives of cell-boundaries are not considered in the former because

Authors are with the Department of Electrical and Computer Engineering, Southern Illinois University, Carbondale, IL, USA 62901, Email: {diluka.lg, rajan.shrestha, gayan.baduge}@siu.edu. This work in part has been presented at Global Communications Conference (Globecom), 2018, Abu Dhabi, UAE [1].

all APs, which are distributed across a given geographical area, cooperatively/coherently serve all user nodes via spatial multiplexing techniques [20]. The TDD-based operation of cell-free massive MIMO enables local estimation of UL channel state estimation (CSI) at each AP [20], and thus, the overhead of CSI exchange among APs can be mitigated. The DL payload data and transmit power allocation coefficients of the user nodes are sent by the CPU to all APs in which a simple maximal ratio transmission (MRT) based precoder can be used for DL transmissions [20]. The APs forward the data received from the user nodes in the UL towards the CPU through the fronthaul/backhaul network. Then, a maximal ratio combining (MRC) based joint detection of UL user signals can be conducted at the CPU by adopting the statistical DL CSI whenever DL channel estimation at the user nodes is utilized to minimize the channel estimation overhead [20]. The benefits of cell-free massive MIMO include high probability of coverage for user nodes with better average channel conditions with average reductions of path-losses, large macro-diversity gains, reduced average transmit power requirements, and large spectral/energy efficiencies [20].

A. SWIPT with co-located massive MIMO

In [26], the maximization of energy efficiency, while satisfying quality-of-service requirement, is investigated for energy beamforming based SWIPT in large-scale MIMO systems. In [27], SWIPT for hybrid data/energy users is studied in the context of massive MIMO by proposing a max-min throughput optimization technique based on optimal allocation of time-slot durations and transmit power. In [28], the performance of SWIPT in DL massive MIMO is investigated by maximizing the minimum harvested energy among the energy-users subject to a minimum achievable rate for the data-users. The performance bounds and power control coefficients of [27] and [28] are valid only for the asymptotically large BS antenna regime. In [29], the impact of imperfectly estimated CSI on SWIPT performance in massive MIMO is studied by quantifying the max-min optimal energy-rate trade-off. In [30], efficient user association techniques for wireless energy transfer in massive MIMO heterogeneous networks are proposed. In [31], [32], the feasibility of adopting dual-hop massive MIMO relay networks in boosting the performance of SWIPT is investigated. In [9], the performance metrics of SWIPT in multi-cell massive MIMO multi-way relay networks are derived in the presence of erroneously estimated CSI.

B. Motivation

Although SWIPT has been extensively adopted for co-located massive MIMO [9], [26]–[29], to the best of our knowledge, practically viable performance bounds of SWIPT for cell-free massive MIMO have not yet been investigated in the open literature except for the initial idea in [33]. Thus, our paper fills this gap by establishing practically achievable performance bounds of SWIPT in cell-free massive MIMO with estimated CSI. The proposed system model can reap benefits of distributed transmission/reception in cell-free massive MIMO to overcome the challenge of low harvested energy levels observed in SWIPT primarily owing to inherent severe path-losses. Since the APs are distributed over a given large geographical area, cell-free massive MIMO leverages macro-diversity benefits to mitigate shadow fading more efficiently than the co-located counterpart. Because the users tend to be located more closer to the APs, SWIPT with cell-free massive MIMO has a potential of offering substantially higher coverage probability, while minimizing the throughput/energy outage probabilities than the co-located massive MIMO. Cell-free massive MIMO has been shown to be more robust against the detrimental correlated small/large-scale fading than the co-located counterpart [20]. Thus, the cell-free massive MIMO can boost the performance of SWIPT, and the underlying practical potential motivates our work.

C. Our contribution

In this paper, we leverage the benefits of cell-free massive MIMO to boost the performance of a hybrid SWIPT/WPT system model. The information and energy are transfered in the DL by adopting SWIPT-enabled cell-free massive MIMO, and then, the DL harvested energy is used for UL user transmissions. Tight approximations to the achievable rates, harvested energy, and fundamental rate-energy trade-offs of SWIPT-enabled cell-free massive MIMO are derived for two PS and TS receiver structures. These performance metrics capture non-linear operating characteristics of the energy harvesting circuitry [14].

Our performance metrics are categorized by considering the availability of statistical CSI and estimated DL CSI at the users. In the former case, the users s rely on statistical CSI for signal decoding, while in the latter case, the estimated DL CSI is used at the users by virtue of DL pilots beamformed by the APs. The energy-rate trade-offs of these two CSI cases are quantified, and our analysis captures the deleterious effects of residual interference caused by beamforming/detection uncertainties at the APs/users owing to imperfect/partial CSI.

This paper technically contributes to the mitigation of detrimental near-far effects on SWIPT performance metrics of a cell-free massive MIMO set-up. The achievable rate-energy trade-offs of the max-min fairness optimal transmit power control are derived to maximize the minimum achievable user rate and the harvested energy for both TS and PS receiver structures. By adopting the corresponding optimal transmit power control coefficients, the common user rates and harvested energies are derived. Then, the max-min fairness optimal energy-rate trade-offs are quantified and compared against those of the uniform power control. Thereby, it is revealed that the proposed power control policies are able to mitigate the near-far effects of SWIPT-enabled cell-free massive MIMO.

Our analysis is then used to quantify the performance gains of SWIPT-enabled cell-free massive MIMO over the conventional co-located counterpart. Consequently, it is shown that the former set-up outperforms the latter mainly owing

to inherent macro-diversity gains and lesser average path-losses caused by distributed APs. However, these gains are achieved by cell-free set-up at the expense of increased back-haul/fronthaul requirements over the co-located counterpart.

Finally, the feasibility of utilizing the energy harvested during the DL SWIPT at the users for UL transmission is investigated by deriving the UL achievable rates. Our analysis reveals that the UL user rate gains for this specific case primarily rely on efficient DL/UL transmit power control. This is because the harvested energy via DL SWIPT depends on DL power control at the APs, while the UL rates depend on how the DL harvested energy is allocated for UL transmit power and battery storage at the users. It is advocated that the transmit power must be jointly controlled to optimize the DL harvested energy and UL achievable rates. The deleterious near-far effects on the energy-rate trade-off for this specific case have shown to be more stringent with the cell-free set-up than the co-located counterpart. Nevertheless, it is also revealed that the proposed max-min power control policies can jointly mitigate near-far effects not only on both DL harvested energy but also DL/UL achievable rates.

D. Difference relative to the existing literature:

Even though there exists a handful of research on SWIPT in co-located massive MIMO [9], [26]–[32], the fundamental performance metrics have not yet been established in the context of SWIPT-enabled cell-free massive MIMO. It has been already shown that the data rate performance of cell-free massive MIMO is fundamentally different from that of the co-located counterpart [20]. Thus, the performance bounds of SWIPT in cell-free massive MIMO are also expected to be considerably different from those established for co-located counterpart [9], [27]–[32]. This is because not only users but also APs are geographically distributed, and hence, the harvested energy and rates are severely hindered by the near-far effects. In [29], max-min transmit power control has been adopted to separately mitigate detrimental near-far effects on the rates and harvested energy in SWIPT-enabled co-located massive MIMO. However, in a cell-free set-up, near-far effects on both the rate and harvested energy must be jointly mitigated. To this end, we investigate max-min transmit power control policies to optimize the energy-rate trade-off, while guaranteeing the user-fairness. The distinct long-term channel coefficients between the distributed APs and the users ensure that our max-min power control solutions are different from those appeared for the co-located counterpart, where the large-scale channel coefficient between a given user and all antennas is the same.

All related prior works on SWIPT-enabled massive MIMO [9], [26]–[32] utilize linear energy harvesting models at the users. Nonetheless, our analysis deviates from this ideal model by adopting a practically viable SWIPT model proposed by [14], which can capture non-linear characteristics of energy harvesting circuitry. Moreover, by adopting a hybrid TS/PS protocol from [35], we generalize our performance analysis for both TS and PS protocols.

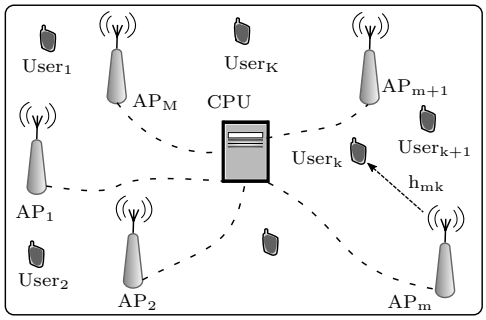


Fig. 1. A cell-free massive MIMO system.

Although the impact of imperfectly estimated UL channels has been investigated to design precoders for SWIPT-enabled massive MIMO [31], [32], the users have been assumed to rely on statistical CSI. This assumption can be justified for co-located massive MIMO because the instantaneous channel coefficients can be approximated tightly by their average counterparts when the number of co-located antennas grows without bound [34]. However, the same justification may not be valid for a cell-free set-up in which the APs are geographically distributed [36]. To this end, distinctively from the related prior research [9], [26]–[32], we investigate the impact of user estimated DL CSI, which is acquired through beamforming DL pilots towards the users, and thereby deriving the SWIPT performance metrics. To the best of our knowledge, the proposed DL/UL max-min fairness optimal energy-rate trade-offs of DL and UL transmission in SWIPT have not yet been reported in the context of cell-free massive MIMO.

Notation: $\mathbf{z}^H$ and $\|\mathbf{z}\|$ denote the conjugate-transpose and Euclidean norm of $\mathbf{z}$, respectively. The conjugate of z is denoted by z^*, and $z \sim \mathcal{CN}(\cdot,\cdot)$ denotes that z is a complex-valued circularly symmetric Gaussian random variable. $\mathbb{E}[\cdot]$ and $\mathbb{V}\mathrm{ar}[\cdot]$ are the expectation and variance, respectively.

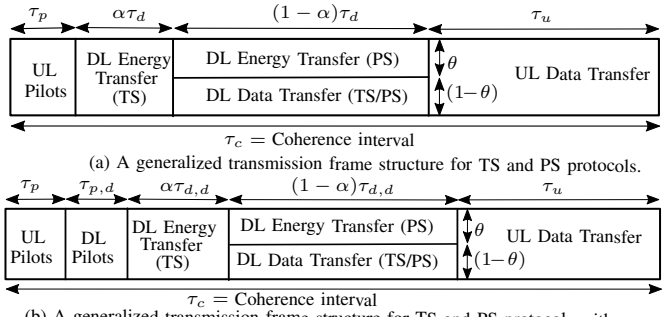
II. System, channel and signal models

A. System model

We consider a TDD-based cell-free massive MIMO system in which M single-antenna APs serve K single-antenna user nodes (see Fig. 1). The user nodes are equipped with both information and energy receivers. The energy harvesting model at each user node is generalized by adopting both TS and PS receiver structures/protocols. The channel coherence interval (τ_c) is divided into three main orthogonal time-slots and used for pilot, DL, and UL transmissions. Depending on the CSI case[1], the pilot phase is used for either only UL and or both UL/DL pilot transmissions (see Fig. 2a and Fig. 2b).

1) SWIPT in DL transmission: The SWIPT is performed in DL transmission phase by using TS protocol, PS protocol or both protocols. Thus, the DL time-slot is further divided into two portions based on the TS/PS factors (α/θ) to receive payload data and harvest the energy. Specifically, $\alpha\tau_d$ portion

[1]The pilot transmission and channel estimation aspects are discussed in Sections II-B1 and VII.



(a) A generalized transmission frame structure for TS and PS protocols.

(b) A generalized transmission frame structure for TS and PS protocols with DL pilot transmission

Fig. 2. A generalized transmission frame structure for TS and PS protocols with/without DL pilots.

of the DL time-slot is dedicated for DL power transfer via TS protocol, while the reminder portion of length $(1-\alpha)\tau_d$ is used for simultaneous DL information transfer. If the PS protocol is adopted, then the received signal power is split into two streams during $(1-\alpha)\tau_d$ via a power splitter having a PS ratio of $\theta : 1-\theta$ and passed through the energy harvester and the information decoder, respectively.

2) UL transmission: The final time-slot (τ_u) of the coherence interval is allocated for the UL[2] user data transmission towards APs. During this UL time-slot, each user node allocates a fraction of its harvested energy in the DL phase for UL data transmission (see Fig. 2a).

3) Backhaul/fronthaul requirement: In cell-free massive MIMO, all APs must be connected to a CPU either via a conventional backhaul network [20] or by using an emerging fronthaul networks in C-RAN [21]. Since the UL channels are estimated locally at each AP via user pilots and a local MRT precoder is employed at each AP, no CSI is exchanged among APs. This considerably reduces the overhead of cell-free systems compared to network MIMO and CoMP. However, DL/UL data must be transmitted to/from the CPU towards APs. Thus, there exists a fundamental trade-off between performance gains and backhaul/fronthaul requirements.

B. Channel model

The channel coefficient between the mth AP and the kth user is denoted by h_{mk}, and the channel is modeled as

$$h_{mk} = \zeta_{mk}^{1/2}\tilde{h}_{mk}, \tag{1}$$

where $\tilde{h}_{mk} \sim \mathcal{CN}(0,1)$ captures small-scale/Rayleigh fading and stays fixed during the coherence interval [34]. Moreover, ζ_{mk} captures the large-scale fading effects, including path-loss and log-normal shadowing, between the mth AP and the kth user. It is typically assumed that these large-scale fading coefficients are known a-priori as they change slowly and remain fixed for thousands of coherence interval [20], [34].

[2]The performance analysis corresponding to joint DL/UL transmission within the same coherence interval is discussed in Section VI.

1) Uplink channel estimation: The UL channels are estimated locally at APs by using user pilots [20]. During the UL time-slot, all K users send pilots of length τ_p to all APs. The pilot transmitted by the kth user is denoted by $\boldsymbol{\phi}_k \in \mathbb{C}^{1\times\tau_p}$, where $k \in \{1,\cdots,K\}$. We assume that these pilots are mutually orthogonal; $\boldsymbol{\phi}_k^H\boldsymbol{\phi}_{k'} = 0$ for $k \neq k'$ and $\|\boldsymbol{\phi}_k\|^2 = 1$. Thus, the pilot length should satisfy $\tau_p \geq K$. The pilot signal received at the mth AP is given by [20], [34]

$$\mathbf{y}'_{pm} = \sqrt{\tau_p P_p}\sum_{k=1}^{K} h_{mk}\boldsymbol{\phi}_k + \mathbf{n}'_m, \tag{2}$$

where P_p is the pilot transmit power of each user, $\mathbf{n}'_m$ is an additive white Gaussian noise (AWGN) vector at the mth AP, and elements of $\mathbf{n}'_m$ are independent and identically distributed (i.i.d.) $\mathcal{CN}(0,1)$ random variables. By projecting (2) onto $\boldsymbol{\phi}_k^H$, a sufficient statistic that can be used to estimate h_{mk} locally at the mth AP can be written as [20], [34]

$$y_{pmk} = \boldsymbol{\phi}_k^H\mathbf{y}'_{pm} = \sqrt{\tau_p P_p}h_{mk} + n_m, \tag{3}$$

where $n_m = \boldsymbol{\phi}_k^H\mathbf{n}'_m \sim \mathcal{CN}(0,1)$ because $\boldsymbol{\phi}_k$ is a unitary vector. The minimum mean square error (MMSE) estimate of h_{mk} can be derived as [37]

$$\hat{h}_{mk} = \frac{\mathbb{E}\left[y^*_{pmk}h_{mk}\right]}{\mathbb{E}[|y_{pmk}|^2]}y_{pmk} = c_{mk}y_{pmk}, \tag{4}$$

where c_{mk} is given by

$$c_{mk} = \frac{\sqrt{\tau_p P_p}\zeta_{mk}}{\tau_p P_p\zeta_{mk}+1}. \tag{5}$$

Due to channel reciprocity property of TDD, APs utilize the same locally estimated $\hat{h}_{mk}$ as DL CSI to construct its precoder [34]. The true channel can be represented as $h_{mk} = \hat{h}_{mk} + \epsilon_{mk}$, where ϵ_{mk} is the estimation error, which is independent of the estimate yielded from the orthogonality property of MMSE criterion [37].

C. Non-linear energy harvesting model

In practice, the harvested energy is a non-linear function of the received power at the rectenna. Such a non-linear energy harvesting circuitry can be modeled as [14]

$$\begin{aligned}\Psi_{EH}(P_R) &= \left[\frac{\lambda}{1-\nu}\left(\frac{1}{1+\exp(-\mu(P_R-\omega))}-\nu\right)\right]^+ \\ &= \left[\frac{\lambda(1-\exp(-\mu P_R))}{1+\exp(-\mu(P_R-\omega))}\right]^+,\end{aligned} \tag{6}$$

where $\Psi_{EH}(P_R)$ is a non-linear function of P_R, and represents the instantaneous harvested energy. Moreover, $\nu = 1/(1+\exp(\mu\omega))$ and $[z]^+ = \max(0,z)$. The non-linearities of the energy harvesting circuitry are modeled via λ, μ and ω. Based on [14], these parameters are set to $\lambda = 20\,\text{mW}$, $\mu = 6400\,/\mu\text{W}$, and $\omega = 2.9\,\mu\text{W}$.

D. Signal model

1) Signal model for DL transmission: In DL transmission, APs employ conjugate precoding, which is designed based on the locally estimated channels (4). The signal transmitted by the mth AP can be written as

$$x_m = \sqrt{P_d}\sum_{k=1}^{K}\eta_{mk}^{1/2}\hat{h}_{mk}^{*}q_k, \tag{7}$$

where q_k is the symbol intended for the kth user satisfying $\mathbb{E}\left[|q_k|^2\right]=1$. In (7), P_d is the maximum allowable transmit power at each AP, and η_{mk} is the power allocation to the kth user symbol at the mth AP. Then, the transmit power constraint of the mth AP can be defined as $\mathbb{E}\left[|x_m|^2\right]\leq P_d$. By substituting (7) into this constraint and applying several mathematical manipulations, it can be rewritten as

$$\sum_{k=1}^{K}\eta_{mk}\mathbb{E}\left[|\hat{h}_{mk}^{*}|^2\right]\leq 1 \quad\Rightarrow\quad \sum_{k=1}^{K}\eta_{mk}\rho_{mk}\leq 1, \tag{8}$$

where $\rho_{mk}\triangleq\mathbb{E}\left[|\hat{h}_{mk}|^2\right]=\sqrt{\tau_p P_p}c_{mk}\zeta_{mk}$. The signal received at the kth user from all M APs can be written as

$$r_k=\sum_{m=1}^{M}h_{mk}x_m+n_k, \tag{9}$$

where $n_k\sim\mathcal{CN}(0,1)$ is an AWGN at the kth user. The signal in (9) can be rearranged as

$$\begin{aligned}r_k=&\sqrt{P_d}\sum_{m=1}^{M}\eta_{mk}^{1/2}h_{mk}\hat{h}_{mk}^{*}q_k\\&+\sqrt{P_d}\sum_{m=1}^{M}\sum_{i\neq k}^{K}\eta_{mi}^{1/2}h_{mk}\hat{h}_{mi}^{*}q_i+n_k,\end{aligned} \tag{10}$$

where the first term represents the desired signal component, while the second term captures the inter-user interference yielded from beamforming uncertainty of conjugate precoding with imperfectly estimated CSI at the APs.

III. Preliminary analysis

A. Instantaneous Harvested Energy

During the first portion of DL time-slot having a length of $\alpha\tau_d$, the APs transfer power in the DL and users harvest energy based on the TS protocol (see Fig. 2a). During the second portion having a length of $(1-\alpha)\tau_d$, users harvest energy based on the PS protocol. The total harvested energy for TS and PS protocols at the kth user can be written as

$$E_k=\alpha\tau_d\Psi_{EH}\left(P_k\right)+(1-\alpha)\tau_d\Psi_{EH}\left(\theta P_k\right), \tag{11}$$

where $\Psi_{EH}(\cdot)$ is the non-linear function in (6), and P_k is the incident/received power at the rectenna of the kth user. By using (9), P_k can be defined as

$$P_k=P_d\left|\sum_{m=1}^{M}\sum_{i=1}^{K}\eta_{mi}^{1/2}h_{mk}\hat{h}_{mi}^{*}q_i\right|^2. \tag{12}$$

Remark 1: The harvested energy (11) can be used to investigate the performance of both TS and PS protocols. By letting $\theta=0$ and $\alpha\neq 0$, the harvested energy yielded by the TS protocol can be computed. If $\alpha=0$ and $\theta\neq 0$, then (11) provides the harvested energy of the PS protocol. When $\alpha\neq 0$ and $\theta\neq 0$, (11) can be used to quantify the performance of a hybrid TS/PS protocol. The same argument applies to the achievable user rate, which is presented in (19).

B. Average Harvested Energy

The average harvested energy at the kth user is given by

$$\bar{E}_k=\alpha\tau_d\mathbb{E}[\Psi_{EH}\left(P_k\right)]+(1-\alpha)\tau_d\mathbb{E}[\Psi_{EH}\left(\theta P_k\right)]. \tag{13}$$

The exact closed-form evaluation of (13) appears mathematically intractable. To obtain useful insights, a tight upper bound for (13) is derived by using Jensen's inequality as

$$\bar{E}_k\leq\bar{E}_k^{ub}=\alpha\tau_d\Psi_{EH}\left(\mathbb{E}[P_k]\right)+(1-\alpha)\tau_d\Psi_{EH}\left(\theta\mathbb{E}[P_k]\right), \tag{14}$$

where $\mathbb{E}[P_k]=\bar{P}_k$ is derived as (see Appendix A)

$$\mathbb{E}[P_k]=P_d\sum_{m=1}^{M}\eta_{mk}\rho_{mk}^2+P_d\sum_{m=1}^{M}\sum_{i=1}^{K}\eta_{mi}\rho_{mi}\zeta_{mk}. \tag{15}$$

C. Achievable DL rate

The users are unaware of instantaneous channel coefficients with no DL pilots, and thus, they must rely on the statistical CSI for the signal decoding [34]. The signal received at the kth user (10) can be re-arranged to be suitable for detection with only statistical channel knowledge at users as given in (16), where $\tilde{P}_d\triangleq P_d\left(1-\theta\right)$. According to [34], [38], the effective noise can be treated as the worst-case independently distributed Gaussian noise. Then, the signal-to-interference-plus-noise ratio (SINR) at the kth user can be written as (17). By computing the expectation and variance terms, this SINR (17) can be derived as (see Appendix B)

$$\gamma_k=\frac{\tilde{P}_d\left(\sum_{m=1}^{M}\eta_{mk}^{1/2}\rho_{mk}\right)^2}{\tilde{P}_d\sum_{m=1}^{M}\sum_{i=1}^{K}\eta_{mi}\rho_{mi}\zeta_{mk}+1}. \tag{18}$$

Then, an achievable rate of the kth user can be defined as

$$R_k=\frac{\left(1-\alpha\right)\tau_d}{\tau_c}\log_2\left(1+\gamma_k\right), \tag{19}$$

where the pre-log factor $\left(1-\alpha\right)\tau_d/\tau_c$ captures the effective potion of the coherence interval for the DL data.

IV. Mitigating near-far effects

Max-min power control has been shown to be optimal in the sense of user-fairness under near-far effects in multi-user systems [34], [39]–[41]. In SWIPT, user-fairness must be guaranteed not only in terms of the rates but also with respect to the harvested energy. In this section, a max-min fairness-based energy-rate trade-off analysis is presented to mitigate the deleterious near-far effects.

$$r_k = \underbrace{\sqrt{\tilde{P}_d}\mathbb{E}\left[\sum_{m=1}^{M}\eta_{mk}^{1/2}h_{mk}\hat{h}_{mk}^{*}q_k\right]}_{\text{desired signal}} + \underbrace{\sqrt{\tilde{P}_d}\left(\sum_{m=1}^{M}\eta_{mk}^{1/2}h_{mk}\hat{h}_{mk}^{*}q_k - \mathbb{E}\left[\sum_{m=1}^{M}\eta_{mk}^{1/2}h_{mk}\hat{h}_{mk}^{*}q_k\right]\right)}_{\text{detection uncertainty}}$$
$$+ \underbrace{\sqrt{\tilde{P}_d}\sum_{m=1}^{M}\sum_{i\neq k}^{K}\eta_{mi}^{1/2}h_{mk}\hat{h}_{mi}^{*}q_i}_{\text{Inter-user interference}} + \underbrace{n_k}_{\text{AWGN}} \tag{16}$$

$$\gamma_k = \frac{\tilde{P}_d\left|\mathbb{E}\left[\sum_{m=1}^{M}\eta_{mk}^{1/2}h_{mk}\hat{h}_{mk}^{*}\right]\right|^2}{\tilde{P}_d\mathbb{V}\mathrm{ar}\left[\sum_{m=1}^{M}\eta_{mk}^{1/2}h_{mk}\hat{h}_{mk}^{*}\right] + \tilde{P}_d\mathbb{E}\left[\left|\sum_{m=1}^{M}\sum_{i\neq k}^{K}\eta_{mi}^{1/2}h_{mk}\hat{h}_{mi}^{*}\right|^2\right] + \mathbb{E}\left[|n_k|^2\right]}, \tag{17}$$

A. Transmit power control for the PS protocol

In PS protocol, the data transmission and energy harvesting take place within the same time-slot, and thus, the transmit power must be controlled jointly to maximize the harvested energy and rate of the weakest user. This requires a multi-objective optimization problem (MOOP) formulation [42]. Thus, this MOOP can be formulated as

$$\underset{\eta_{mk}\forall m,k}{\text{maximize}} \quad \left(\bar{R}_{c,PS}\right)^{w_r}\left(\bar{E}_{c,PS}\right)^{w_e} = \lambda_c \tag{20a}$$
$$\text{subject to } C_1 : R_k^{w_r}\bar{E}_k^{w_e} \geq \lambda_c, \tag{20b}$$
$$C_2 : \sum_{k=1}^{K}\eta_{mk}\rho_{mk} \leq 1, \tag{20c}$$
$$C_3 : 0 \leq \eta_{mk}, \tag{20d}$$

where $\bar{R}_{c,PS}$ and $\bar{E}_{c,PS}$ are the system-wide common target DL rate and the harvested energy, respectively. Moreover, w_r and w_e are the priorities assigned to $\bar{R}_{c,PS}$ and $\bar{E}_{c,PS}$, respectively. Due to the non-convex nature of the multi-objective function in (20b) [43], an optimal closed-form solution to this MOOP becomes mathematically intractable for a finite number of APs[3]. To circumvent this difficulty, a two-step approach is proposed to obtain the max-min optimal energy-rate trade-off for PS protocol. In the first step, by keeping the PS factor fixed, a common harvested energy is obtained by maximizing the minimum harvested energy. In the second step, a common DL user rate can be derived by maximizing the minimum user rate for a fixed PS factor. The common rate and harvested energy are functions of the PS factor. By solving for the PS factor from the common rate and then by substituting it to the common harvested energy, a max-min fairness-based energy-rate trade-off can be derived.

1) Maximizing minimum harvested energy for PS protocol: A max-min power control policy is formulated to maximize the minimum harvested energy for a fixed PS factor as

$$\underset{\eta_{mk}\forall m,k}{\text{maximize}} \quad \bar{E}_{c,PS} \tag{21a}$$
$$\text{subject to } C_1 : \bar{E}_k \geq \bar{E}_{c,PS}, \tag{21b}$$
$$C_2 : \sum_{k=1}^{K}\eta_{mk}\rho_{mk} \leq 1, \tag{21c}$$
$$C_3 : 0 \leq \eta_{mk}, \tag{21d}$$

where $\bar{E}_{c,PS}$ is the common target for the harvested energy and $\bar{E}_k$ is given in (14) with $\alpha = 0$ for the PS protocol. As per (14), $\bar{E}_k$ is a non-decreasing function of the average received power, and thus, $\bar{E}_k$ can be replaced by $\mathbb{E}[P_k]$, which is given in (15). Next, the max-min optimization problem in (21) can be equivalently reformulated by defining a slack variable $\beta_{mk} \triangleq \eta_{mk}^{1/2}$ as

$$\underset{\beta_{mk}\forall m,k}{\text{maximize}} \quad \bar{P}_{c,PS} \tag{22a}$$
$$\text{subject to } C_1 : \mathbb{E}[P_k] \geq \bar{P}_{c,PS}, \tag{22b}$$
$$C_2 : \sum_{k=1}^{K}\beta_{mk}^2\rho_{mk} \leq 1, \tag{22c}$$
$$C_3 : 0 \leq \beta_{mk}, \tag{22d}$$

where $\bar{P}_{c,PS}$ is the common average received power. The constraints (22b)-(22d) and the objective function (22a) are convex [44]. This convex optimization problem (22) can be modeled as a second order cone programming (SOCP) and solved via CVX [44].

Algorithm 1 The proposed statistical channel information based pilot assignment and user grouping algorithm

Input: Path-losses between all M APs and K users and the average transmit power, P_d.

Output: The power control coefficients η_{mk} for $m \in \{1, \cdots, M\}$ and $k \in \{1, \cdots, K\}$.

1: Begin - CVX.
2: Set a common target average received power, $\bar{P}_{c,PS}$.
3: Solve the convex feasibility problem given by

$$\|\boldsymbol{V}_{E_k}\| \geq \sqrt{\bar{P}_{c,PS}/P_d}, \tag{23}$$

which is subjected to the constraints (22c)-(22d). Moreover, $\|\boldsymbol{V}_{E_k}\| \triangleq \left[\mathbf{v}_{E1}^T, \mathbf{v}_{E2}^T\right]$, where $\mathbf{v}_{E1}$ and $\mathbf{v}_{E2}$ are given by

$$\mathbf{v}_{E1} \triangleq \left[\beta_{1k}\rho_{1k}, \cdots, \beta_{Mk}\rho_{Mk}\right]^T, \tag{24a}$$
$$\mathbf{v}_{E2} \triangleq \left[\beta_{11}\sqrt{\rho_{11}\zeta_{1k}}, \cdots, \beta_{MK}\sqrt{\rho_{MK}\zeta_{Mk}}\right]^T. \tag{24b}$$

4: End - CVX.
5: **return** $\eta_{mk} = \beta_{mk}^2$ for $m \in \{1, \cdots, M\}$ and $k \in \{1, \cdots, K\}$.

2) Maximizing minimum achievable rate for PS protocol: By invoking the max-min optimization [34], the optimal transmit power control coefficients can be computed for a

[3]This MOOP is solved in the large AP regime as shown in Section V-A.

fixed PS factor to maximize the minimum DL rate among all users. To this end, a max-min power control problem can be formulated by replacing $\bar{E}_{c,PS}$ and $\bar{E}_k$ in (21) with $\bar{R}_{c,PS}$, the common/target DL rate that can be achieved at the optimal solution and R_k, the instantaneous DL rate of the kth user given in (19) with $\alpha = 0$, respectively.

Since R_k is a non-decreasing function of its argument, the kth user rate can be replaced by the SINR of the kth user (γ_k), which is given in (18). By introducing a common SINR ($\gamma_{c,PS}$) for all users and by defining a slack variable $\beta_{mk} \triangleq \eta_{mk}^{1/2}$, the optimization problem can be equivalently reformulated as

$$\underset{\beta_{mk}\forall m,k}{\text{maximize}} \quad \gamma_{c,PS} \tag{25a}$$

$$\text{subject to } C_1 : \gamma_k \geq \gamma_{c,PS}, \tag{25b}$$

$$C_2 : \sum\nolimits_{k=1}^{K} \beta_{mk}^2 \rho_{mk} \leq 1, \tag{25c}$$

$$C_3 : 0 \leq \beta_{mk}. \tag{25d}$$

Since the objective function in (25a) is a quasi-concave function, the underlying optimization problem is also quasi-concave [20], [44]. Then, an optimal solution for the feasibility problem in (25) for a fixed PS factor (θ) can be obtained by invoking a variation of the Bisection method for solving SOCP [20], [44] as presented in Algorithm 2.

3) Max-min optimal energy-rate trade-off for PS protocol: By first solving for θ in (21b) and then substituting it into (25b), a max-min fairness-based common energy-rate trade-off for PS protocol can be obtained by using the max-min optimal solutions of $\bar{P}^*_{c,PS}$ and $\gamma^*_{c,PS}$ as in (26).

Remark 2: Any point along this energy-rate trade-off curve (26) corresponds to a common harvested energy and user rate pair computed via solving max-min fairness-based optimization. Then, the PS factor (θ) for any point along this trade-off curve can be obtained via back-substitution of either common harvested energy or user rate into the corresponding metric, which is in turn a function of the PS factor.

B. Transmit power control for the TS protocol

In this subsection, our objective is to mitigate the adverse near-far effects of SWIPT with TS protocol, in which the power and information transfers occur in two orthogonal time-slots. Thus, the transmit power can be optimized to ensure max-min user-fairness in terms of both harvested energy and user rates for a given TS factor. Thereby, the max-min fairness optimal energy-rate trade-off can be derived. By traversing through this trade-off curve, a max-min optimal TS factor (α) for any common energy-rate can be obtained.

1) Max-min fairness optimal common harvested energy for TS protocol: In this subsection, a common harvested energy at each user is obtained via max-min transmit power control. Since all users achieve this common harvested energy for a given TS factor, the near-far effect can be readily mitigated. Since the harvested energy is a non-decreasing function of the average received power, the max-min optimal power control coefficients can be computed by setting a common received energy ($\bar{E}_{c,TS}$) for every user. Thus, a max-min power control policy to ensure a common harvested energy can be formulated by replacing the $\bar{E}_{c,PS}$ and $\bar{E}_k$ in (21) with $\bar{E}_{c,TS}$ and $\mathbb{E}[P_k]$, defined in (15), respectively. The objective function of the optimization problem can shown to be convex [34], [44]. The equality of the respective optimization problem holds at the optimal solution, and thus, all harvested energies must be equal to the common maximum value, $\bar{E}^*_{c,TS}$. Then, the optimization problem can be reformulated and then solved by adopting an algorithm similar to one used for (22) by using CVX [44].

2) Max-min fairness optimal common user rate for TS protocol: A max-min fairness common rate for a fixed TS factor (α) can be obtained by computing transmit power allocation coefficients to maximize the minimum DL user rates among all users [34]. The user rate in (19) is a non-decreasing function of the SINR, γ_k. Thus, by introducing a common SINR ($\gamma_{c,TS}$) for all users, the power control coefficients can be computed such that this common SINR is maximized. Then, by keeping the TS factor fixed, a max-min power control policy can be formulated by replacing $\gamma_{c,PS}$ in (25) with $\gamma_{c,TS}$. Since the objective function is quasi-concave, this optimization problem too becomes quasi-concave [20], [44]. Then, this can be solved via the same Bisection method [44] proposed for (25).

Algorithm 2 : Bisection algorithm for transmit power control

Input: Path-losses between all M APs and K users and the average transmit power, P_d.

Output: The power control coefficients η_{mk} for $m \in \{1, \cdots, M\}$ and $k \in \{1, \cdots, K\}$.

Initialization: Define an initial region for the objective functions by choosing appropriate values for t_{min} and t_{max}. Choose a tolerance $\epsilon > 0$.

1: **while** $t_{max} - t_{min} > \epsilon$ **do**

2: Calculate, $\gamma_{c,PS} = (t_{max} + t_{min})/2$.

3: Solve the convex feasibility problem, which can be given as

$$\|\boldsymbol{V}_{\gamma_k}\| \leq \frac{1}{\sqrt{\gamma_{c,PS}}} \left(\sum\nolimits_{m=1}^{M} \beta_{mk} \rho_{mk} \right), \tag{27}$$

which is subjected to C_2 and C_3 given in (25c) and (25d), respectively. Moreover, $\boldsymbol{V}_{\gamma_k} \triangleq \left[\mathbf{v}_1^T, \ 1/\sqrt{\bar{P}_d} \right]$, where

$$\mathbf{v}_1 \triangleq [\beta_{11}\sqrt{\rho_{11}}, \cdots, \beta_{MK}\sqrt{\rho_{MK}}]^T. \tag{28}$$

4: If the status of the problem is feasible, then set $t_{min} = \gamma_{c,PS}$, otherwise set $t_{max} = \gamma_{c,PS}$.

5: Stop if $t_{max} - t_{min} < \epsilon$. Otherwise go to Step 2.

6: **end while**

7: **return** $\eta_{mk} = \beta_{mk}^2$ for $m \in \{1, \cdots, M\}$ and $k \in \{1, \cdots, K\}$.

$$R^*_{c,PS} = \frac{\tau_d}{\tau_c}\log_2\left(1+\frac{P_d\left(1-\bar{E}^*_{c,PS}\Psi^{-1}_{EH}\left(\bar{P}^*_{c,PS}\right)/\tau_d\right)\left(\sum_{m=1}^{M}\eta_{mk}^{1/2}\rho_{mk}\right)^2}{P_d\left(1-\bar{E}^*_{c,PS}\Psi^{-1}_{EH}\left(\bar{P}^*_{c,PS}\right)/\tau_d\right)\sum_{m=1}^{M}\sum_{i=1}^{K}\eta_{mi}\rho_{mi}\zeta_{mk}+1}\right) \tag{26}$$

$$R^*_{c,TS} = \frac{\left(1-\bar{E}^*_{c,TS}\Psi^{-1}_{EH}\left(\bar{P}^*_{c,TS}\right)/\tau_d\right)\tau_d}{\tau_c}\log_2\left(1+\frac{P_d\left(\sum_{m=1}^{M}\eta_{mk}^{1/2}\rho_{mk}\right)^2}{P_d\sum_{m=1}^{M}\sum_{i=1}^{K}\eta_{mi}\rho_{mi}\zeta_{mk}+1}\right) \tag{29}$$

3) Max-min optimal energy-rate trade-off for TS protocol: The max-min optimal energy-rate trade-off for the TS protocol can be derived by first solving for α in (14) and then by substitute it into (19). Thus, the max-min optimal energy-rate trade-off for the TS protocol can be written as (29).

Remark 3: By traversing through the energy-rate trade-off curve in (29), the max-min optimal TS factor for any pair of common energy and rate can be obtained. The TS factor (α) is a function of the energy harvesting duration within a coherence interval. Thus, our solution inherently deals with optimizing the time-slots allocated for energy harvesting and data transmission in the sense of max-min user-fairness.

V. Asymptotic Analysis for DL transmission

In this section, the performance of SWIPT is investigated when the number of APs grows without bound ($M \to \infty$). By substituting the UL channel estimate in (3) and (4) into (10), an asymptotic approximation for the received power at the kth user can be derived as (see Appendix D)

$$P_{k,\infty} = P_d\left(\sum_{m=1}^{M}\eta_{mk}^{1/2}\rho_{mk}\right)^2. \tag{30}$$

The asymptotic harvested energy at the kth user is given by

$$\bar{E}_k = \alpha\tau_d\Psi_{EH}\left(\mathbb{E}[P_{k,\infty}]\right) + (1-\alpha)\tau_d\Psi_{EH}\left(\theta\mathbb{E}[P_{k,\infty}]\right). \tag{31}$$

The asymptotic achievable rate at the kth user is given by

$$R_{k,\infty} = \frac{(1-\alpha)\,\tau_d}{\tau_c}\log_2\left(1+\gamma_{k,\infty}\right), \tag{32}$$

where the asymptotic SINR ($\gamma_{k,\infty}$) is given by

$$\gamma_{k,\infty} = \tilde{P}_d\left(\sum_{m=1}^{M}\eta_{mk}^{1/2}\rho_{mk}\right)^2, \tag{33}$$

where the receiver noise variance is normalized to unity.

A. Asymptotic transmit power control for PS protocol

In contrast to Section IV-A, in this subsection, a MOOP [42] is formulated to control transmit power in the asymptotic AP regime ($M \to \infty$). This MOOP formulation is particularly useful for the PS protocol in which the energy and data transfer take place in the same time slot. Thus, a MOOP is formulated to asymptotically optimize the energy-rate trade-off of PS protocol as [42]

$$\underset{\beta_{mk}\forall m,k}{\text{maximize}} \quad \left(P^{\infty}_{c,PS}\right)^{w_e}\left(\gamma^{\infty}_{c,PS}\right)^{w_r} = \lambda \tag{34a}$$

$$\text{subject to } C_1: \sqrt{\lambda} \le \sqrt{P_d}\left(\sum\nolimits_{m=1}^{M}\beta_{mk}\rho_{mk}\right), \tag{34b}$$

$$C_2: \sum\nolimits_{k=1}^{K}\beta^2_{mk}\rho_{mk} \le 1, \tag{34c}$$

$$C_3: 0 \le \beta_{mk}, \tag{34d}$$

where w_e and w_r are the priorities assigned for the harvested energy and rate. For instance, if energy and data transfers have the same priority, then $w_e = w_r = 1$ [29], [42]. In (34b), $\beta_{mk} \triangleq \eta_{mk}^{1/2}$ and λ is a slack variable for the common rate and harvested energy. All constraints and objective function in (34) are convex [34], [44]. Consequently, the MOOP in (34) is solved via CVX [44].

At the optimal solution, by solving for θ in the harvested energy in (31) and then substituting it into the user rate in (33), the asymptotically optimal energy-rate trade-off is derived as (35).

B. Asymptotic transmit power control for TS protocol

Since the energy and data transmissions take place in two orthogonal time-slots in the TS protocol, the two separate max-min problems to optimize the harvested energy and achievable rate can be formulated by following steps similar to (34). For the energy transfer phase of the TS protocol, λ in the objective function in (34) becomes the common harvested energy with unity priority; $w_e = 1$ ($w_r = 0$). For the data transfer phase, λ in the objective function in (34) must be replaced by the common achievable rate with unity priority; $w_r = 1$ ($w_e = 0$). These optimization problems can be shown to be convex and hence can be solved via CVX [44].

By following a similar approach to the PS protocol, at the optimal solution, we derive the asymptotic max-min optimal energy-rate trade-off as $M \to \infty$ as in (36).

VI. Uplink Transmission

A. Signal model for UL transmission

In UL, the users are typically assumed to be equipped with an external back-up power source in the event that the harvested energy level is inadequate for sending UL data in a mission critical application [3], [4]. Thus, the total energy at the kth user can be written as

$$E^{Tot}_k = E^{Rem}_k + \bar{E}_k, \tag{37}$$

$$R_{c,PS}^{\infty *} = \frac{\tau_d}{\tau_c}\log_2\left(1+\left(1-E_{c,PS}^{\infty *}\Psi_{EH}^{-1}\left(P_{c,PS}^{\infty *}\right)/\tau_d\right)P_d\left(\sum_{m=1}^{M}\eta_{mk}^{1/2}\rho_{mk}\right)^2\right) \tag{35}$$

$$R_{c,TS}^{\infty *} = \frac{\left(1-E_{c,TS}^{\infty *}\Psi_{EH}^{-1}\left(P_{c,TS}^{\infty *}\right)/\tau_d\right)\tau_d}{\tau_c}\log_2\left(1+P_d\left(\sum_{m=1}^{M}\eta_{mk}^{1/2}\rho_{mk}\right)^2\right) \tag{36}$$

where E_k^{Rem} is the back-up/remaining energy at the kth user and $\bar{E}_k$ is the total harvested energy (13). We also defined a threshold energy, E_k^{Min}, which is the minimum energy that is needed for pilot transmission at the kth user. Then, the kth user transmits its UL signal if

$$E_k^{Min} > (1-\kappa)E_k^{Tot}, \tag{38}$$

where $0 < \kappa < 1$ is a fraction used to allocate transmit power between the UL payload data and pilots. Then, a predefined portion of this total energy can be used for UL payload data transfer at each user, while the remaining portion can be used for UL pilot transfer. The average transmit power used for UL data transfer at the kth user can be derived as

$$P_{uk} = \kappa E_k^{Tot}/\tau_u, \tag{39}$$

where τ_u is the coherence interval allocated for UL data transmission, and E_k^{Tot} is the total available energy defined in (37). The signal received at the mth AP can be written as

$$r_{m,u} = \sum_{k=1}^{K}\sqrt{P_{uk}\eta_k}h_{mk}q_{k,u} + n_{m,u}, \tag{40}$$

where $q_{k,u}$ is the signal transmitted by the kth user satisfying $\mathbb{E}\left[|q_{k,u}|^2\right] = 1$, η_k is its UL power control coefficient and $n_{m,u} \sim \mathcal{CN}(0,1)$ is an AWGN at the mth AP. Then, the mth AP employs a conjugate precoder, which is constructed based on its local UL channel estimate (4). The post-processed signal at the CPU from the kth user can be written as

$$r_{k,u} = \sum_{m=1}^{M}\hat{h}_{mk}^{*}r_{m,u}, \tag{41}$$

where $r_{m,u}$ is given in (40). By substituting (40) into (41), the received signal at the CPU can be rewritten as

$$r_{k,u} = \sum_{m=1}^{M}\sqrt{P_{uk}\eta_k}\hat{h}_{mk}^{*}h_{mk}q_{k,u} + \sum_{m=1}^{M}\hat{h}_{mk}^{*}n_{m,u} + \sum_{m=1}^{M}\sum_{i\neq 1}^{K}\sqrt{P_{ui}\eta_i}\hat{h}_{mk}^{*}h_{mi}q_{i,u}, \tag{42}$$

where the first, second, and third terms represent the desired signal component, filtered noise and, inter-user interference.

B. The UL achievable rate

By following steps similar to (16), the received signal (42) can be rearranged to make it suitable for decoding at the CPU as (43). By using (43), the effective UL SINR can be derived as (44). The variance and expectation terms of (44) can be computed by using techniques similar to those in Appendix B. Thereby, the UL SINR can be derived in closed-form as

$$\gamma_{k,u} = \frac{P_{uk}\eta_k\left(\sum_{m=1}^{M}\rho_{mk}\right)^2}{\sum_{i=1}^{K}P_{ui}\eta_i\sum_{m=1}^{M}\rho_{mk}\zeta_{mi} + \sum_{m=1}^{M}\rho_{mk}}. \tag{45}$$

Next, we derive the achievable UL rate as follows:

$$R_{k,u} = \frac{\tau_u}{\tau_c}\log_2\left(1+\gamma_{k,u}\right), \tag{46}$$

where τ_u/τ_c captures the effective potion of the coherence interval used for UL data transfer and $\gamma_{k,u}$ is defined in (45).

C. Joint DL/UL transmit power control

To ensure that the UL user rates are independent of the near-far effects, while maximizing the minimum DL harvested energy, a joint max-min fairness optimal DL/UL transmit power control problem is formulated. Thus, at the optimal solution of this joint power control, all users achieve a common UL rate regardless of their channel conditions, while satisfying a common DL harvested energy constraint for all users. The achievable rate in (46) is a monotonically increasing function of its argument $\gamma_{k,u}$. Since the non-convexity of non-linear energy harvesting model in (6), we adopted linear energy harvesting model only for calculating UL transmit powers in the joint optimization problem. By first introducing a common UL SINR ($\gamma_{c,u}$) and a common DL harvested energy ($E_{c,d}$) for all users and then by defining slack variables $\beta_k \triangleq \eta_k^{1/2}$ and $\beta_{mk} \triangleq \eta_{mk}$, a max-min joint power control problem can be formulated as

$$\underset{\beta_{mk},\beta_k\forall m,k}{\text{maximize}} \quad (E_{c,d})^{w_e}(\gamma_{c,u})^{w_r} \tag{47a}$$

subject to

$$C_1 : \mathbb{E}[P_k] \geq E_{c,d}, \tag{47b}$$

$$C_2 : \|\boldsymbol{V}_{\gamma_{k,u}}\| \leq \frac{1}{\sqrt{\gamma_{c,u}}}\left(\sum\nolimits_{m=1}^{M}\beta_k\rho_{mk}\right), \tag{47c}$$

$$C_3 : \sum\nolimits_{k=1}^{K}\beta_{mk}\rho_{mk} \leq 1, \quad \text{and} \quad 0 \leq \beta_{mk} \leq 1, \tag{47d}$$

$$C_4 : \sum\nolimits_{k=1}^{K}\beta_k^2\rho_{mk} \leq 1, \quad \text{and} \quad 0 \leq \beta_k \leq 1, \tag{47e}$$

where $\boldsymbol{V}_{\gamma_{k,u}} \triangleq \left[\mathbf{v}_{1,u}^T,\ \mathbf{v}_{2,u}^T\right]$. Moreover, $\mathbf{v}_{1,u}$ and $\mathbf{v}_{2,u}$ are given by

$$\mathbf{v}_{1,u} \triangleq \left[\beta_1\sqrt{\frac{P_{u1}\rho_{1k}\zeta_{11}}{P_{uk}}}, \cdots, \beta_K\sqrt{\frac{P_{uK}\rho_{Mk}\zeta_{MK}}{P_{uk}}}\right]^T, \tag{48a}$$

$$\mathbf{v}_{2,u} \triangleq \left[\sqrt{\rho_{1k}/P_{uk}}, \cdots, \sqrt{\rho_{Mk}/P_{uk}}\right]^T. \tag{48b}$$

Since the objective function in (47a) is quasi-concave, this optimization problem is also quasi-concave [20], [44]. Thus,

the optimization problem in (47) can be solved as a CVX [44] feasible problem by using Algorithm 3. Since both energy and rate are equally prioritized in SWIPT, we set the weights in (47a) to $w_e = w_r = 1$ [42].

Algorithm 3 : Bisection algorithm for DL/UL power control

Input: Path-loss coefficients between all M APs and K users, the average transmit powers of the users, and UL energy conversion efficiencies of the users.

Output: The DL power control coefficients η_{mk} for $m \in \{1, \cdots, M\}$, $k \in \{1, \cdots, K\}$ and the UL power control coefficients η_k for $k \in \{1, \cdots, K\}$.

Stage 1:

1: Begin - CVX.

2: Set a common target value for harvested energy.

3: Solve the convex feasible problem given by

$$\|\boldsymbol{V}_{E_k}\| \geq \sqrt{E_{c,d}/P_d}, \tag{49}$$

which is subjected to the constraint (47d). $\|\boldsymbol{V}_{E_k}\| \triangleq \left[\mathbf{v}_{E1}^T,\ \mathbf{v}_{E2}^T\right]$, where $\mathbf{v}_{E1}$ and $\mathbf{v}_{E2}$ are given in (24).

4: Compute the UL transmit power of the user via DL power control coefficients (β_{mk}^*) by assuming that only harvested energy is used for UL data transmission

$$P_{uk}^* = \Omega \left(\sum_{m=1}^{M} \beta_{mk}^* \rho_{mk}^2 + \sum_{m=1}^{M} \sum_{i=1}^{K} \beta_{mi}^* \rho_{mi} \zeta_{mk} \right), \tag{50}$$

where $\Omega \triangleq \kappa \tau_d \left(\alpha + (1-\alpha)\theta\right) P_d / \tau_u$.

Stage 2:

5: By using Algorithm 2, solve the the convex feasible problem given by

$$\|\boldsymbol{V}_{\gamma_{k,u}}\| \leq \frac{1}{\sqrt{\gamma_{c,u}}} \left(\sum_{m=1}^{M} \beta_k \rho_{mk} \right), \tag{51}$$

which is subjected to (47e). Further, $\boldsymbol{V}_{\gamma_{k,u}} \triangleq \left[\mathbf{v}_{1,u}^T,\ \mathbf{v}_{2,u}^T\right]$, where $\mathbf{v}_{1,u}$ and $\mathbf{v}_{2,u}$ are given in (48b).

6: End - CVX.

7: **return** $\eta_{mk} = \beta_{mk}$ for $m \in \{1, \cdots, M\}$ and $k \in \{1, \cdots, K\}$ and $\eta_k = \beta_k^2$ for $k \in \{1, \cdots, K\}$.

D. Computational complexity

The convex optimization problems in (22), (25), (34), and (47) are typically solved as SOCP via Matlab CVX [44]. Thus, the computational complexity in terms of the number of arithmetic operations to solve the corresponding SOCP can be given as $\mathcal{O}(n_v^2 n_c)$, where n_v is the number of optimization variables and n_c is the number of second order cone constraints [45]. The total number of iteration required for solving the Bisection method is given by $\log_2\left([t_{max} - t_{min}]/2\right)$ [44], where t_{max} and t_{min} are defined in Algorithm 2. Thus, these computational complexities are furnished in Table I.

TABLE I
COMPUTATIONAL COMPLEXITY OF THE PROPOSED ALGORITHMS IN TERMS OF THE NUMBER OF ARITHMETIC OPERATIONS

Algorithm	Number of arithmetic operations
Algorithm 1	$\mathcal{O}(M^2K^3)$
Algorithm 2	$\log_2\left([t_{max} - t_{min}]/2\right) \times \mathcal{O}(M^2K^3)$
Algorithm 3	$\log_2\left([t_{max} - t_{min}]/2\right) \times \mathcal{O}(M^2K^3)^2$

VII. The implications of DL pilot transmission and DL channel estimates at users

Thus far, the users have been assumed to be unaware of DL channel estimates, and the DL channel statistics have been used for signal decoding by assuming that the effective DL channel coefficients can be approximated by their average counterparts by virtue of channel hardening property of massive MIMO [34]. For co-located massive MIMO, channel hardening has been justified [38]. Nevertheless, it has been shown in [36] that the channel hardening in cell-free massive MIMO occurs only in scenarios where a very large number of APs is deployed in close vicinity. To circumvent this, in cell-free massive MIMO, the DL channels can be estimated at the users via DL pilots beamformed by APs, and the estimated DL CSI can be used for signal decoding. Here, we present a performance analysis of SWIPT with DL pilots.

A. Downlink channel estimation at users

Having been locally estimated UL channels, the APs can now beamform the DL pilots towards the users. This technique guarantees that the DL pilot sequence length depends only on the number of users, and it does not scale with the number of APs [20], [36]. This technique thus paves a way of efficiently estimating DL channels at the user nodes, while preserving the system scalability.

Based on the first term of (16), the effective DL channel coefficient that must be estimated by the kth user node to decode its desired signal is given by

$$a_{ki} \triangleq \sum_{m=1}^{M} \eta_{mi}^{1/2} h_{mk} \hat{h}_{mi}^*. \tag{52}$$

The DL pilot length is $\tau_{p,d}$ in symbol durations (see Fig.2b). Thus, an additional $\tau_{p,d}$ duration is needed for DL channels estimation.

The pilot sequence transmitted by the mth AP is denoted by $\boldsymbol{\phi}_{k,d} \in \mathbb{C}^{\tau_{p,d} \times 1}$, where $k \in \{1, \cdots, K\}$. These DL pilots are also mutually orthogonal, satisfying $\boldsymbol{\phi}_{k,d}^H \boldsymbol{\phi}_{k',d} = 0$ for $k \neq k'$ and $\|\boldsymbol{\phi}_{k,d}\|^2 = 1$. The pilot signal sent by the mth AP can be then written as

$$\mathbf{x}_{pm} = \sqrt{\tau_{p,d} P_{p,d}} \sum_{k=1}^{K} \eta_{mk}^{1/2} \hat{h}_{mk}^* \boldsymbol{\phi}_{k,d}, \tag{53}$$

where $P_{p,d}$ is the DL pilot transmit power at each AP, and $\hat{h}_{mk}$ is defined in (4). The pilot vector received at the kth user can be written as

$$\mathbf{y}'_{k,d} = \sum_{m=1}^{M} h_{mk} \mathbf{x}_{pm} + \mathbf{n}'_{pk,d}, \tag{54}$$

$$r_{k,u} = \underbrace{\mathbb{E}\left[\sum_{m=1}^{M}\sqrt{P_{uk}\eta_k}\hat{h}_{mk}^{*}h_{mk}q_{k,u}\right]}_{\text{desired signal}} + \underbrace{\left(\sum_{m=1}^{M}\sqrt{P_{uk}\eta_k}\hat{h}_{mk}^{*}h_{mk}q_{k,u} - \mathbb{E}\left[\sum_{m=1}^{M}\sqrt{P_{uk}\eta_k}\hat{h}_{mk}^{*}h_{mk}q_{k,u}\right]\right)}_{\text{detection uncertainty}}$$
$$+ \underbrace{\sum_{m=1}^{M}\sum_{i\neq k}^{K}\sqrt{P_{ui}\eta_i}\hat{h}_{mk}^{*}h_{mi}q_{i,u}}_{\text{Inter-user interference}} + \underbrace{\sum_{m=1}^{M}\hat{h}_{mk}^{*}n_{m,u}}_{\text{AWGN}} \tag{43}$$

$$\gamma_{k,u} = \frac{\left|\mathbb{E}\left[\sum_{m=1}^{M}\sqrt{P_{uk}\eta_k}\hat{h}_{mk}^{*}h_{mk}\right]\right|^2}{\mathbb{V}\mathrm{ar}\left[\sum_{m=1}^{M}\sqrt{P_{uk}\eta_k}\hat{h}_{mk}^{*}h_{mk}\right] + \mathbb{E}\left[\left|\sum_{m=1}^{M}\sum_{i\neq k}^{K}\sqrt{P_{ui}\eta_i}\hat{h}_{mk}^{*}h_{mi}\right|^2\right] + \mathbb{E}\left[\left|\sum_{m=1}^{M}\hat{h}_{mk}^{*}n_{m,u}\right|^2\right]} \tag{44}$$

$$r_{k,d} = \underbrace{\sqrt{\tilde{P}_d}\mathbb{E}[(a_{kk}|\hat{a}_{kk})]\,q_k}_{\text{desired signal}} + \underbrace{\sqrt{\tilde{P}_d}\left((a_{kk}|\hat{a}_{kk})\,q_k - \mathbb{E}[(a_{kk}|\hat{a}_{kk})]\,q_k\right)}_{\text{detection uncertainty}} + \underbrace{\sqrt{\tilde{P}_d}\sum\nolimits_{i\neq k}^{K}(a_{ki}|\hat{a}_{kk})\,q_i}_{\text{Inter-user interference}} + \underbrace{n_{k,d}}_{\text{AWGN}} \tag{61}$$

$$\mathbb{E}_{\hat{a}_{kk}}[\gamma_{k,d}] = \frac{\sum_{m=1}^{M}\sum_{m'=1}^{M}\eta_{mk}^{1/2}\eta_{m'k}^{1/2}\rho_{mk}\rho_{m'k} + \sum_{m=1}^{M}\eta_{mk}\zeta_{mk}\rho_{mk} - \frac{v_{kk}}{\tau_{p,d}P_{p,d}v_{kk}+1}}{P_d\frac{v_{kk}}{\tau_{p,d}P_{p,d}v_{kk}+1} + P_d\sum_{i\neq k}^{K}\sum_{m=1}^{M}\eta_{mi}\zeta_{mk}\rho_{mi} + 1} \tag{67}$$

where $\mathbf{n}'_{pk,d} \sim \mathcal{CN}(\mathbf{0}, \mathbf{I})$ is the kth user AWGN vector. The received pilot signal is rewritten by using (53) and (54) as

$$\mathbf{y}'_{k,d} = \sqrt{\tau_{p,d}P_{p,d}}\sum_{i=1}^{K}a_{ki}\boldsymbol{\phi}_{i,d} + \mathbf{n}'_{pk,d}, \tag{55}$$

where a_{ki} is the effective DL channel and is defined in (52). A sufficient statistic to estimate this effective DL channel can be obtained by projecting (55) into $\boldsymbol{\phi}_{k,d}$ as

$$y_{k,d} = \boldsymbol{\phi}_{k,d}^{H}\mathbf{y}'_{k,d} = \sqrt{\tau_{p,d}P_{p,d}}a_{kk} + n_{pk,d}, \tag{56}$$

where $n_{pk,d} = \boldsymbol{\phi}_{k,d}^{H}\mathbf{n}'_{pk,d}$. By using (56), the MMSE estimate of the effective channel coefficient (a_{kk}) is derived as [36]

$$\hat{a}_{kk} = \mathbb{E}[a_{kk}] + \frac{\sqrt{\tau_{p,d}P_{p,d}}\mathbb{V}\mathrm{ar}[a_{kk}]}{\tau_{p,d}P_{p,d}\mathbb{V}\mathrm{ar}[a_{kk}] + 1}\left(y_{k,d} - \sqrt{\tau_{p,d}P_{p,d}}\mathbb{E}[a_{kk}]\right). \tag{57}$$

By evaluating $\mathbb{V}\mathrm{ar}[a_{kk}]$ and $\mathbb{E}[a_{kk}]$, the MMSE estimate of a_{kk} can be derived as (see Appendix A in [36])

$$\hat{a}_{kk} = \frac{\sqrt{\tau_{p,d}P_{p,d}}v_{kk}y_{k,d} + \sum_{m=1}^{M}\eta_{mk}^{1/2}\rho_{mk}}{\tau_{p,d}P_{p,d}v_{kk} + 1}, \tag{58}$$

where v_{kk} is defined as

$$v_{kk} \triangleq \sum_{m=1}^{M}\eta_{mk}\zeta_{mk}\rho_{mk}. \tag{59}$$

The actual effective DL channel coefficient is given by $a_{kk} = \hat{a}_{kk} + \epsilon_{kk}^{a}$, where ϵ_{kk}^{a} is an estimation error, which is independent of $\hat{a}_{kk}$ [37].

B. Achievable DL rate with DL pilots/channel estimates

The received signal at the kth user (10) can be rewritten by using the effective DL channel coefficient (52) as

$$r_{k,d} = \sqrt{P_d}a_{kk}q_k + \sqrt{P_d}\sum_{i\neq k}^{K}a_{ki}q_i + n_{k,d}, \tag{60}$$

where $n_{k,d} \sim \mathcal{CN}(0,1)$ is the kth user AWGN. When DL channel estimates are available at the kth user, (60) can be rearranged for signal decoding as (61) [36], [46]. By using (61), the SINR can be written as

$$\gamma_{k,d} = \frac{\tilde{P}_d|\mathbb{E}[a_{kk}|\hat{a}_{kk}]\,|^2}{\tilde{P}_d\sum_{i=1}^{K}\mathbb{E}\left[|a_{ki}|^2|\hat{a}_{kk}\right] - \tilde{P}_d|\mathbb{E}[a_{kk}|\hat{a}_{kk}]\,|^2 + 1}. \tag{62}$$

By noticing that a_{kk} is Gaussian distributed, and the pairs $(\hat{a}_{kk}, \epsilon_{kk}^{a})$ and (a_{kk}, a_{ki}) are independent for $k \neq i$, the SINR in (62) can be rewritten as follows:

$$\gamma_{k,d} = \frac{\tilde{P}_d|\hat{a}_{kk}|^2}{\tilde{P}_d\sum_{i\neq k}^{K}\mathbb{E}[|a_{ki}|^2] + \tilde{P}_d\mathbb{E}[|\epsilon_{kk}^{a}|^2] + 1}. \tag{63}$$

Then, the achievable DL rate can be defined as

$$R_{k,d} = \frac{(1-\alpha)\,\tau_{d,d}}{\tau_c}\mathbb{E}_{\hat{a}_{kk}}[\log_2(1+\gamma_{k,d})], \tag{64}$$

where $\tau_{d,d} = \tau_c - (\tau_p + \tau_{p,d} + \tau_u)$. By invoking Jensen's inequality, an upper bound of the DL rate at the kth user node can be derived as

$$R_{k,d}^{ub} = \frac{(1-\alpha)\,\tau_{d,d}}{\tau_c}\log_2(1 + \mathbb{E}_{\hat{a}_{kk}}[\gamma_{k,d}]), \tag{65}$$

where $\mathbb{E}_{\hat{a}_{kk}}[\gamma_{k,d}]$ is given by

$$\mathbb{E}_{\hat{a}_{kk}}[\gamma_{k,d}] = \frac{\tilde{P}_d\mathbb{E}\left[|\hat{a}_{kk}|^2\right]}{\tilde{P}_d\mathbb{E}[|\epsilon_{kk}^{a}|^2] + \tilde{P}_d\sum_{i\neq k}^{K}\mathbb{E}[|a_{ki}|^2] + 1}. \tag{66}$$

By evaluating expectation terms in (66), the effective SINR can be written as in (67) (see Appendix C for derivation).

VIII. Numerical Results

The path-loss between the mth AP and the kth user is modeled as $\zeta_{mk} = (d_0/d_{mk})^{\nu} \times 10^{\varphi_{mk}/10}$, where d_{mk} is the distance between the mth AP and the kth user, d_0 is the reference distance, ν is the path-loss exponent, and $10^{\varphi_{mk}/10}$

$$F_{\mathcal{R}_{\min}}(\mathcal{R}) = \mathrm{P_r}\left(\mathcal{R}_{\min} = \min_k \left(\frac{(1-\alpha)\,\tau_d}{\tau_c}\log_2\left(1+\gamma_k\right)\right) \leq \mathcal{R}\right) \tag{68}$$

$$F_{\mathcal{E}_{\min}}(\mathcal{E}) = \mathrm{P_r}\left(\mathcal{E}_{\min} = \min_k \left(\alpha\tau_d\Psi_{EH}\left(P_k\right) + (1-\alpha)\tau_d\Psi_{EH}\left(\theta P_k\right)\right) \leq \mathcal{E}\right) \tag{69}$$

captures log-normal shadow fading with $\varphi_{mk} \sim \mathcal{N}(0, \sigma_{sh}^2)$ [34]. The APs are uniformly distributed, while the user nodes are randomly distributed over an area of $D \times D\,\mathrm{m}^2$. Other simulation parameters are tabulated in Table II.

TABLE II
SYSTEM PARAMETERS FOR THE SIMULATIONS

Parameter	value
Carrier frequency	2 GHz
Bandwidth	20 MHz
Noise figure	10 dB
Noise variance	-91 dBm
D, d_0	300 m, 1 m
σ_{sh}^2	8 dB
τ_c, $\tau_p = \tau_{p,d}$	196, K
ν	3.4

In Fig. 3, the harvested energy curves for TS and PS protocols are plotted against the average transmit power ($\bar{\gamma}$) by using linear and non-linear SWIPT models. The curves for the finite and infinite AP regimes are plotted via Monte-Carlo simulations and our asymptotic analysis (30), respectively. The harvested energy of non-linear SWIPT model (6) is compared to that of the linear model with a fixed RF-to-DC conversion efficiency of 0.9. Fig. 3 reveals that the linear SWIPT model overwhelmingly overestimates the harvested energy with respect to the non-linear counterpart in medium-to-high average transmit power regime. Fig. 3 also depicts that the harvested energy can be boosted by increasing the density of distributed APs in a given geographical area. For instance with PS protocol, at an average transmit power of 5 mW, the harvested energy can be improved by 69.4% when the number of APs is increased from 64 to 484. The PS protocol outperforms TS protocol because the former is able to perform energy harvesting during the entire DL time-slot via power-splitters, while the latter employs time-division technique, which is typically sub-optimal.

In Fig. 4, the energy-rate trade-offs of co-located and cell-free massive MIMO are compared. In the former case, the BS is equipped with an $M = 64$ antenna array, while the same number of APs is uniformly distributed in the latter case. User locations are fixed for both systems. These trade-off curves are plotted by using (13) and (19) with $\alpha = 0$ and $\theta = 0$ for PS and TS protocols, respectively. Fig. 4 confirms that the distributed APs outperform the co-located counterpart. For example, at a sum rate of 1.5 bits/s/Hz, the cell-free massive MIMO provides harvested energy gains of 71.4% and 33.7%, respectively, for TS and PS protocols, over the co-located massive MIMO. However, cell-free set-up achieves this performance gain at the expense of an additional backhaul/fronthaul requirement. Moreover, Fig. 4 depicts the fundamental trade-off between the harvested energy and the sum rate. On one hand, the sum rate is maximized when the

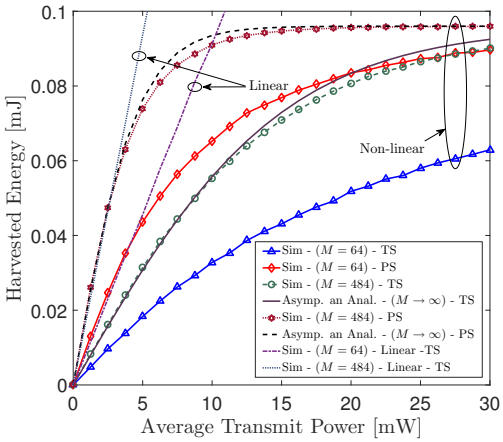


Fig. 3. The harvested energy versus the average transmit power for TS and PS protocols for $\alpha = 0.5$, $\theta = 0.5$.

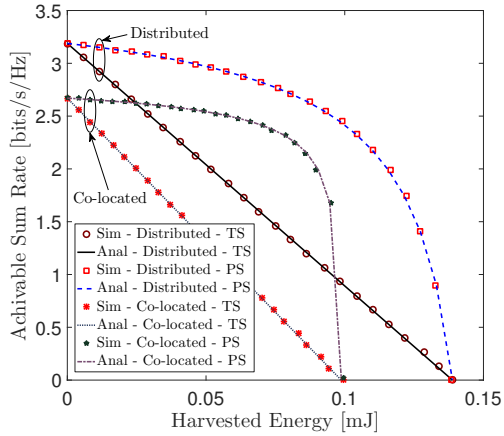


Fig. 4. A comparison of the energy-rate trade-off between the distributed and co-located massive MIMO architectures of TS and PS protocols for $M = 64$, $K = 2$ and $\bar{\gamma} = 10\,\mathrm{dBm}$.

both TS and PS factors approach zero, and at this operating point, the entire time-slot allocated for the DL is used only for data transfer. Simultaneously, the harvested energies at the users become infinitesimal. On the other hand, the harvested energy becomes a maximum when the TS and PS factors approach unity, and consequently at this operating point, the sum rate vanishes. Thus, by traversing through the energy-rate trade-off curves in Fig. 4, the harvested energies and sum rates can be obtained for any given TS/PS factor.

In Fig. 5 and Fig. 6, the performance of the proposed max-min fairness-based transmit power control is compared against the uniform power control. To this end, the cumulative distribution functions (CDFs) of the minimum user rate and minimum user harvested energy pertaining to PS protocol are plotted in Fig. 5 and Fig. 6, respectively, by varying the number of APs as $M = 64$ and $M = 144$. These CDFs are evaluated as given in (68) and (69), where $\mathrm{P_r}(\cdot)$ denotes the probability operator. This comparison reveals the

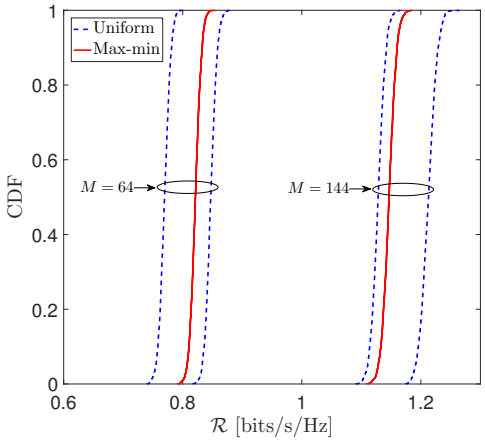


Fig. 5. The CDF of the minimum achievable user rate of PS protocol for $K = 2$, $\bar{\gamma} = 10$ dBm and $\theta = 0.5$.

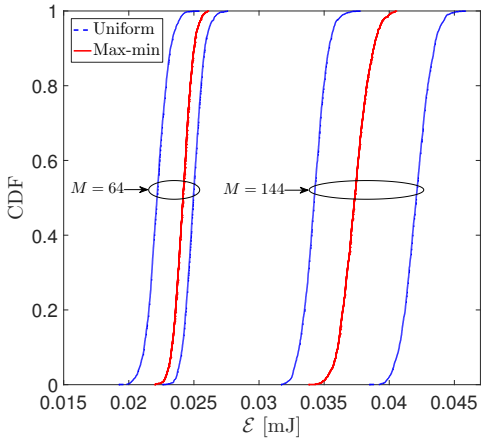


Fig. 6. The CDF of the minimum user harvested energy of PS protocol for $K = 2$, $\bar{\gamma} = 10$ dBm and $\theta = 0.5$.

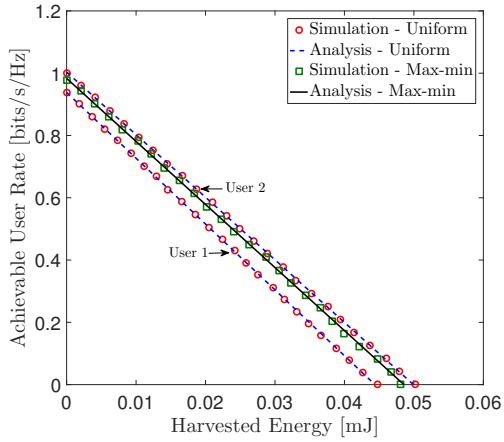


Fig. 7. The energy-rate trade-off of TS protocol for $K = 2$ and $\bar{\gamma} = 10$ dBm, and $M = 64$.

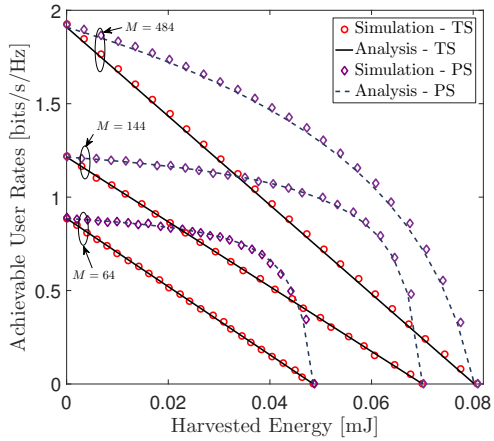


Fig. 8. A comparison of the energy-rate trade-off with different number of APs for $K = 2$ and $\bar{\gamma} = 10$ dBm..

performance gains that can be acquired by adopting the proposed max-min power control over the uniform counterpart. For instance as per Fig. 5, at $M = 64$, the 90%-likely user rate of the max-min power control is about 0.807 bits/s/Hz, which is in turn 1.08 times higher than that of the uniform power control, which provides a minimum user rate about 0.757 bits/s/Hz at the same operating point. Similarly, Fig. 6 reveals that the max-min power control renders a 1.09 times gain in terms of the 90%-likely harvested energy over the uniform counterpart at $M = 64$. Fig. 5 and Fig. 6 also reveal that the 90%-likely user rate and harvested energy can be boosted by 1.41 and 1.56 times, respectively, when the number of APs is increased from $M = 64$ to $M = 144$. Thus, the proposed max-min power control guarantees to enhance the user rate and harvested energy with weak channel conditions.

In Fig. 7, the achievable energy-rate trade-off of the TS protocol is investigated. By using the optimal solutions of the proposed max-min transmit power control policies in section IV-B2, the max-min fairness optimal/common energy-rate trade-off (29) is plotted. The noise at the kth user's receiver is modeled as AWGN[4] with variance, $\sigma_n^2 = -91$ dBm. The energy-rate trade-offs of individual users with a uniform power control policy are also plotted for comparison purposes. Fig. 7 reveals that users experience distinct energy-rate trade-offs when the uniform power control is adopted, and thus, the underlying performance metrics are dependent on the detrimental near-far effects. However, once the proposed max-min power control is employed, all users achieve a common energy-rate trade-off regardless of near-far effects.

In Fig. 8, the impacts of number of APs on the energy-rate trade-offs of TS and PS protocols are studied. Three sets of trade-off curves are plotted by changing the number of APs as $M \in \{64, 144, 484\}$. We observe from Fig. 8 that the energy-rate trade-off can be boosted significantly by increasing the AP density in a given geographical area. For instance, at a harvested energy of 0.02 mJ, the system with $M = 144$ APs achieves a sum rate gain of 64% over the system with $M = 64$ for TS protocol. The asymptotic ($M \to \infty$) energy-rate trade-off curves are plotted by using (31) and (32). The Monte-Carlo simulation with $M = 484$ matches well with the asymptotic analysis in (31) and (32). Thus, the asymptotic performance limits can be obtained in practice with large but finite AP regime.

In Fig. 9 and Fig. 10, the joint effects of the hybrid TS and PS protocol are investigated by plotting the sum rate (19) and harvested energy (13), respectively, as a function of TS

[4]The noise variance in dBm, $\sigma_n^2 = -174 + 10\log_2(B) + N_f$, where $B = 20$ MHz is the channel bandwidth and $N_f = 10$ dB is the noise figure of the receiver.

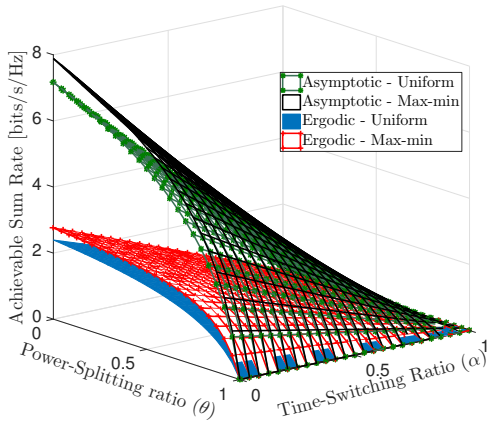


Fig. 9. The achievable sum rate as a function of the TS and PS factors for for $K = 2$ and $\bar{\gamma} = 10$ dBm.

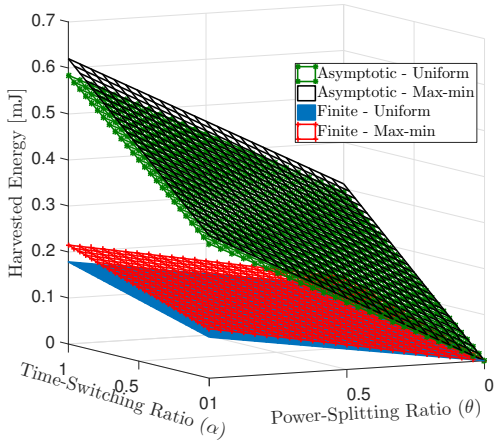


Fig. 10. The total harvested energy as a function of the TS and PS factors for for $K = 2$ and $\bar{\gamma} = 10$ dBm.

(α) and PS (θ) factors. The max-min fairness optimal rate for PS protocol is plotted by adopting the optimal solution of (25). Moreover, for PS protocol, the max-min optimization for the harvested energy (22) is adopted. When both α and θ approach unity, the sum rate becomes infinitesimal (see Fig. 9), whereas the harvested energy becomes a maximum (see Fig. 10). Moreover, Fig. 9 and Fig. 10 reveal impact of the number of APs on the corresponding performance metrics.

In Fig. 11, the performance of the proposed joint DL/UL transmit power control is investigated by plotting the UL user rate as a function of the DL harvested energy by varying the average DL transmit power. The harvested energy in the DL (i.e., (39) with $\kappa = 0.85$) is used for UL transmission. Specifically, the DL harvested energy versus UL rate trade-off of the proposed max-min fairness based joint transmit power control is compared with that of the uniform counterpart. The max-min optimal curve is plotted by solving the optimization problem in (47). Fig. 11 shows that the joint max-min power control yields a common trade-off between the DL energy and UL rate regardless of the distributed nature of APs/users and thus, preserving the user-fairness in terms of the DL energy harvesting and UL user rates. However, the same trade-off is adversely effected when the uniform power control is adopted owing to the inherent near-far effects in a cell-free massive MIMO set-up.

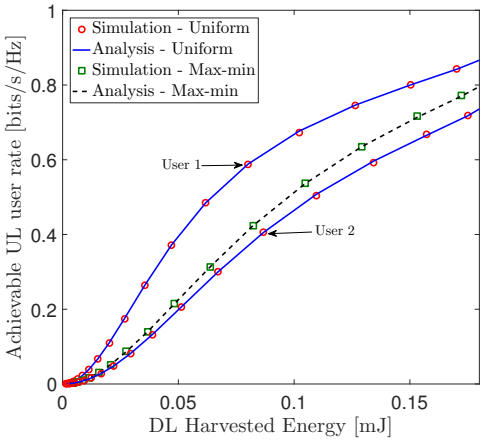


Fig. 11. Achievable UL user rate versus DL harvested energy for $M = 64$, $K = 2$, $\alpha = 0.5$ and $\theta = 0.5$.

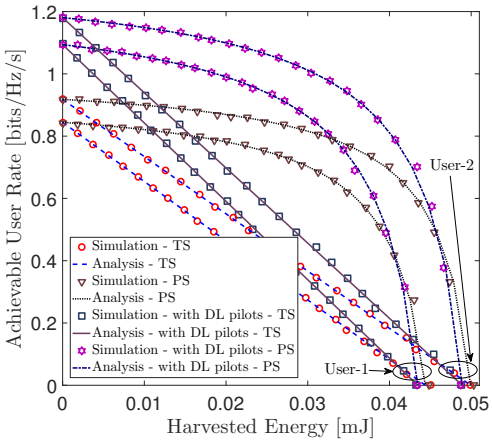


Fig. 12. A comparison of the energy-rate trade-off with/without DL pilots for $M = 64$, $K = 2$, and $\bar{\gamma} = 10$ dBm.

In Fig. 12, the impact of DL pilots on the energy-rate trade-off is investigated for both TS and PS protocols by using Monte-Carlo simulations and our analysis in (66) and (67). Fig. 12 clearly revels that when the estimated CSI, which is facilitated by beamforming DL pilots, is utilized at the users for signal decoding instead of relying on statistical CSI, the achievable rate can be boosted substantially. Since the task of beamforming DL pilots requires an additional time-slot of length $\tau_{p,d}$, which is otherwise be used for energy harvesting purposes, the harvested energy is affected detrimentally. Thus, Fig. 12 shows that the harvested energy of the case with DL pilots is slightly less than that of the case without DL pilots. Nevertheless, as per Fig. 12, the user rate gain acquired through enabling estimated DL CSI at users via beamforming DL pilots is more prominent than the slight degradation of the harvested energy. Thus, the use of DL pilots is useful in enhancing the overall energy-rate trade-off of SWIPT operated in a cell-free massive MIMO set-up.

IX. Conclusion

The benefits of leveraging cell-free massive MIMO in practically realizing SWIPT have been investigated. The feasibility of utilizing a portion of DL harvested energy in UL user transmissions has been explored by deriving the UL user rates. By adopting a non-linear energy harvesting

model, locally estimated UL CSI at the APs and statistical CSI at the users, tight approximations to the harvested energies, achievable user rates, and energy-rate trade-offs have been derived. The impact of DL channel estimation at users via DL pilot beamfoming to boost the energy-rate trade-off has been studied. We reveal that user fairness in terms of both harvested energy and rates can be guaranteed by adopting max-min based transmit power control policies. By deriving the max-min optimal energy-rate trade-offs, we reveal that a common harvested energy and user rate at any given TS/PS factor can be achieved for all users regardless of near-far effects. By deriving max-min optimal power control coefficients for the UL, we show that the detrimental effects of near-far effect on the UL user rates can also be mitigated. We reveal that the linear energy harvesting model overestimates the SWIPT performance over those of the non-linear counterpart. Through a max-min energy-rate trade-off comparison, we conclude that a cell-free massive MIMO set-up can potentially boost the SWIPT performance over a co-located counterpart at the expense of additional backhaul/fronthaul requirements.

Appendix A
Derivation of $\mathbb{E}[P_k]$ in (15)

By substituting (4) and (12) into (15), the average received power can be derived as

$$\begin{aligned}\mathbb{E}[P_k] &= P_d\mathbb{E}\left[\left|\sum_{m=1}^{M}\eta_{mk}^{1/2}h_{mk}\hat{h}_{mk}^{*}\right|^2\right] \\ &+P_d\mathbb{E}\left[\left|\sum_{m=1}^{M}\sum_{i\neq k}^{K}\eta_{mi}^{1/2}h_{mk}\hat{h}_{mi}^{*}\right|^2\right] \\ &= P_d\sum_{m=1}^{M}\eta_{mk}c_{mk}^2\zeta_{mk}\left(2\tau_p P_p\zeta_{mk}+1\right) \\ &+P_d\sum_{m=1}^{M}\sum_{i\neq k}^{K}\eta_{mi}c_{mi}^2\zeta_{mk}\left(\tau_p P_p\zeta_{mi}+1\right) \\ &= P_d\sum_{m=1}^{M}\eta_{mk}\rho_{mk}^2+P_d\sum_{m=1}^{M}\sum_{i=1}^{K}\eta_{mi}\rho_{mi}\zeta_{mk}.\end{aligned} \tag{70}$$

Furthermore, ρ_{mk} in (15) can be derived as

$$\begin{aligned}\rho_{mk} &= \mathbb{E}\left[\left|\hat{h}_{mk}\right|^2\right] = c_{mk}^2\mathbb{E}\left[\left|y_{pmk}\right|^2\right] \\ &= c_{mk}\mathbb{E}\left[\left(\sqrt{\tau_p P_p}h_{mk}^{*}+n_m\right)h_{mk}\right] = \sqrt{\tau_p P_p}c_{mk}\zeta_{mk}.\end{aligned} \tag{71}$$

Appendix B
Derivation of SINR in (18)

The expectation in numerator of (17) can be derived as

$$\begin{aligned}\mathbb{E}\left[\sum_{m=1}^{M}\eta_{mk}^{1/2}h_{mk}\hat{h}_{mk}^{*}\right] &= \sum_{m=1}^{M}\eta_{mk}^{1/2}\mathbb{E}\left[\left(\hat{h}_{mk}+\epsilon_{mk}\right)\hat{h}_{mk}^{*}\right] \\ &= \sum_{m=1}^{M}\eta_{mk}^{1/2}\mathbb{E}\left[\hat{h}_{mk}\hat{h}_{mk}^{*}\right] = \sum_{m=1}^{M}\eta_{mk}^{1/2}\rho_{mk},\end{aligned} \tag{72}$$

where ϵ_{mk} is the error of MMSE estimate of h_{mk} such that $h_{mk}=\hat{h}_{mk}+\epsilon_{mk}$. Then, the variance in (17) is derived as

$$\begin{aligned}&\mathbb{V}\mathrm{ar}\left[\sum_{m=1}^{M}\eta_{mk}^{1/2}h_{mk}\hat{h}_{mk}^{*}\right] \\ &= \sum_{m=1}^{M}\eta_{mk}\left(\mathbb{E}\left[\left|\left(\hat{h}_{mk}+\epsilon_{mk}\right)\hat{h}_{mk}^{*}\right|^2\right]-\rho_{mk}^2\right) \\ &= \sum_{m=1}^{M}\eta_{mk}\left(2\rho_{mk}^2+\rho_{mk}\left(\zeta_{mk}-\rho_{mk}\right)-\rho_{mk}^2\right) \\ &= \sum_{m=1}^{M}\eta_{mk}\rho_{mk}\zeta_{mk}.\end{aligned} \tag{73}$$

The expectation in denominator of (17) can be computed as

$$\begin{aligned}&\mathbb{E}\left[\left|\sum_{i\neq k}^{K}\sum_{m=1}^{M}\eta_{mi}^{1/2}h_{mk}\hat{h}_{mi}^{*}\right|^2\right] \\ &\overset{(a)}{=}\sum_{i\neq k}^{K}\sum_{m=1}^{M}\eta_{mi}c_{mi}^2\mathbb{E}\left[\left|h_{mk}y_{pmi}\right|^2\right] \\ &\overset{(b)}{=}\sum_{i\neq k}^{K}\sum_{m=1}^{M}\eta_{mi}c_{mi}^2\zeta_{mk}\left(\tau_p P_p\zeta_{mi}+1\right) \\ &=\sum_{i\neq k}^{K}\sum_{m=1}^{M}\eta_{mi}\rho_{mi}\zeta_{mk},\end{aligned} \tag{74}$$

where the steps (a) and (b) are written by substituting (3) and (4) into (4) and (17), respectively.

Appendix C
Derivation of effective SINR in (67)

Next, $\mathbb{E}\left[\left|\epsilon_{kk}^{a}\right|^2\right]$ in (66) is computed by substituting (58) and (56) into the expectation of the denominator in (66) as

$$\begin{aligned}\mathbb{E}\left[\left|\epsilon_{kk}^{a}\right|^2\right] &= \mathbb{E}\left[\left|a_{kk}-\hat{a}_{kk}\right|^2\right] \\ &= \mathbb{E}\left[\left|\frac{a_{kk}-\sum_{m=1}^{M}\eta_{mk}^{1/2}\rho_{mk}-\sqrt{\tau_{p,d}P_{p,d}}v_{kk}n_{pk,d}}{\tau_{p,d}P_{p,d}v_{kk}+1}\right|^2\right] \\ &= \frac{\mathbb{E}\left[\left|a_{kk}-\mathbb{E}[a_{kk}]-\sqrt{\tau_{p,d}P_{p,d}}v_{kk}n_{pk,d}\right|^2\right]}{\left(\tau_{p,d}P_{p,d}v_{kk}+1\right)^2} \\ &= \frac{\mathbb{V}\mathrm{ar}[a_{kk}]+\tau_{p,d}P_{p,d}v_{kk}^2}{\left(\tau_{p,d}P_{p,d}v_{kk}+1\right)^2} = \frac{v_{kk}}{\left(\tau_{p,d}P_{p,d}v_{kk}+1\right)}.\end{aligned} \tag{75}$$

The second expectation term in the denominator of (66) can be derived as

$$\begin{aligned}\mathbb{E}\left[\left|a_{ki}\right|^2\right] &= \mathbb{E}\left[\left|\sum_{m=1}^{M}\eta_{mi}^{1/2}\hat{h}_{mk}\hat{h}_{mi}^{*}\right|^2\right] \\ &+\mathbb{E}\left[\left|\sum_{m=1}^{M}\eta_{mi}^{1/2}\epsilon_{mk}\hat{h}_{mi}^{*}\right|^2\right] = \sum_{m=1}^{M}\eta_{mi}\zeta_{mk}\rho_{mi}.\end{aligned} \tag{76}$$

The expectation term in the numerator of (66) is given by

$$\mathbb{E}\left[\left|\hat{a}_{kk}\right|^2\right] = \mathbb{E}\left[\left|a_{kk}-\epsilon_{kk}^{a}\right|^2\right] = \mathbb{E}\left[\left|a_{kk}\right|^2\right]-\mathbb{E}\left[\left|\epsilon_{kk}^{a}\right|^2\right]. \tag{77}$$

By substituting (30) in [36] and (75) into (77), we have

$$\mathbb{E}\left[|\hat{a}_{kk}|^2\right] = \sum_{m=1}^{M}\sum_{m'=1}^{M}\eta_{mk}^{1/2}\eta_{m'k}^{1/2}\rho_{mk}\rho_{m'k} + \sum_{m=1}^{M}\eta_{mk}\zeta_{mk}\rho_{mk} - \frac{v_{kk}}{\tau_{p,d}P_{p,d}v_{kk}+1}. \quad (78)$$

Then, by substituting (75), (77) and (78) into (66), the DL rate with DL pilots can be derived as shown in (67).

APPENDIX D
DERIVATION OF ASYMPTOTIC SIGNAL POWER

As $M \to \infty$, the received signal power at the kth user can be given as

$$P_{k,\infty} = |r_{k,\infty}|^2 = \lim_{M\to\infty}|r_k|^2 = \lim_{M\to\infty}\left|\sqrt{P_d}\sum_{m=1}^{M}\sum_{i=1}^{K}\eta_{mi}^{1/2}h_{mk}\hat{h}_{mi}^{*}q_i\right|^2, \quad (79)$$

where r_k is given in (10). By using channel estimate in (4), and then, by invoking Tchebyshev's theorem [47], we have

$$\frac{1}{M}\sum_{m=1}^{M}\eta_{mi}^{1/2}h_{mk}\hat{h}_{mi}^{*} - \frac{1}{M}\sqrt{\tau_p P_p}\sum_{m=1}^{M}\eta_{mi}^{1/2}c_{mi}\zeta_{mk}\boldsymbol{\phi}_i^T\boldsymbol{\phi}_k^{*} \underset{M\to\infty}{\to} 0. \quad (80)$$

Since we use orthogonal pilots with $\boldsymbol{\phi}_i^T\boldsymbol{\phi}_k^{*} = 0$ for $i \neq k$, the residual interference due to pilot contamination disappears from the received signal. Thus, we have

$$\frac{r_k}{M} - \frac{\sqrt{\tau_p P_p P_d}}{M}\sum_{m=1}^{M}\eta_{mk}^{1/2}c_{mk}\zeta_{mk}q_k \underset{M\to\infty}{\to} 0. \quad (81)$$

Then, the signal received at the kth user can be asymptotically approximated as

$$r_{k,\infty} = \lim_{M\to\infty} r_k \to \sqrt{\tau_p P_p P_d}\sum_{m=1}^{M}\eta_{mk}^{1/2}c_{mk}\zeta_{mk}q_k. \quad (82)$$

Thus, the received signal at the kth user can be written when $M \to \infty$ as

$$r_{k,\infty} = \sqrt{\tau_p P_p P_d}\sum_{m=1}^{M}\eta_{mk}^{1/2}c_{mk}\zeta_{mk}q_k = \sqrt{P_d}\sum_{m=1}^{M}\eta_{mk}^{1/2}\rho_{mk}q_k. \quad (83)$$

By substituting (83) into (79), the power of the received signal can be derived as

$$P_{k,\infty} = |r_{k,\infty}|^2 = P_d\left(\sum_{m=1}^{M}\eta_{mk}^{1/2}\rho_{mk}\right)^2. \quad (84)$$

REFERENCES

[1] R. Shrestha and G. Amarasuriya Aruma Baduge, "SWIPT in Cell-Free Massive MIMO," in *Proc. IEEE Global Commun. Conf. (GLOBECOM)*, Dec. 2018.

[2] J. Lin *et al.*, "A Survey on Internet of Things: Architecture, Enabling Technologies, Security and Privacy, and Applications," vol. 4, no. 5, pp. 1125–1142, Oct 2017.

[3] D. W. K. Ng, E. S. Lo, and R. Schober, "Wireless Information and Power Transfer: Energy Efficiency Optimization in OFDMA Systems," *IEEE Trans. Wireless Commun.*, vol. 12, no. 12, pp. 6352–6370, December 2013.

[4] Q. Yao, T. Q. S. Quek, A. Huang, and H. Shan, "Joint Downlink and Uplink Energy Minimization in WET-Enabled Networks," *IEEE Trans. Wireless Commun.*, vol. 16, no. 10, pp. 6751–6765, Oct 2017.

[5] L. R. Varshney, "Transporting Information and Energy Simultaneously," in *Proc. IEEE Int. Symp. Info. Theory (ISIT)*, Jul. 2008, pp. 1612–1616.

[6] R. Zhang and C. K. Ho, "MIMO Broadcasting for Simultaneous Wireless Information and Power Transfer," *IEEE Trans. Wireless Commun.*, vol. 12, no. 5, pp. 1989–2001, May 2013.

[7] H. J. Visser and R. J. M. Vullers, "RF Energy Harvesting and Transport for Wireless Sensor Network Applications: Principles and Requirements," *Proc. IEEE*, vol. 101, no. 6, pp. 1410–1423, June 2013.

[8] Z. Ding *et al.*, "Application of Smart Antenna Technologies in Simultaneous Wireless Information and Power Transfer," *IEEE Commun. Mag.*, vol. 53, no. 4, pp. 86–93, April 2015.

[9] G. Amarasuriya, E. G. Larsson, and H. V. Poor, "Wireless Information and Power Transfer in Multiway Massive MIMO Relay Networks," *IEEE Trans. Wireless Commun.*, vol. 15, no. 6, pp. 3837–3855, June 2016.

[10] T. D. P. Perera, D. N. K. Jayakody, S. K. Sharma, S. Chatzinotas, and J. Li, "Simultaneous Wireless Information and Power Transfer (SWIPT): Recent Advances and Future Challenges," *IEEE Commun. Surveys Tuts.*, vol. 20, no. 1, pp. 264–302, Firstquarter 2018.

[11] A. A. Nasir, X. Zhou, S. Durrani, and R. A. Kennedy, "Relaying Protocols for Wireless Energy Harvesting and Information Processing," *IEEE Trans. Wireless Commun.*, vol. 12, no. 7, pp. 3622–3636, Jul. 2013.

[12] I. Krikidis, S. Sasaki, S. Timotheou, and Z. Ding, "A Low Complexity Antenna Switching for Joint Wireless Information and Energy Transfer in MIMO Relay Channels," *IEEE Trans. Commun.*, vol. 62, no. 5, pp. 1577–1587, May 2014.

[13] J. A. Hagerty, F. B. Helmbrecht, W. H. McCalpin, R. Zane, and Z. B. Popovic, "Recycling Ambient Microwave Energy with Broad-band Rectenna Arrays," *IEEE Trans. Microw. Theory Tech.*, vol. 52, no. 3, pp. 1014–1024, Mar. 2004.

[14] S. Wang, M. Xia, K. Huang, and Y. Wu, "Wirelessly Powered Two-Way Communication with Nonlinear Energy Harvesting Model: Rate Regions Under Fixed and Mobile Relay," *IEEE Trans. Wireless Commun.*, vol. 16, no. 12, pp. 8190–8204, Dec. 2017.

[15] Y. Wang, Y. Wang, F. Zhou, Y. Wu, and H. Zhou, "Resource Allocation in Wireless Powered Cognitive Radio Networks Based on a Practical Non-Linear Energy Harvesting Model," vol. 5, pp. 17 618–17 626, 2017.

[16] T. L. Marzetta, "Noncooperative Cellular Wireless with Unlimited Numbers of Base Station Antennas," *IEEE Trans. Wireless Commun.*, vol. 9, no. 11, pp. 3590–3600, Nov. 2010.

[17] Sprint Unveils Six 5G-Ready Cities; Significant Milestone Toward Launching First 5G Mobile Network in the U.S. [Online]. Available: https://newsroom.sprint.com/sprint-unveils-5G-ready-massive-MIMO-markets.htm,accessed: 03-05-19.

[18] 3GPP, *NR;Physical Channels and Modulation (Release 15)*, 2019-03.

[19] H. Q. Ngo, A. Ashikhmin, H. Yang, E. G. Larsson, and T. L. Marzetta, "Cell-Free Massive MIMO: Uniformly Great Service for Everyone," in *2015 IEEE 16th International Workshop on Signal Processing Advances in Wireless Communications (SPAWC)*, Jun. 2015, pp. 201–205.

[20] ——, "Cell-Free Massive MIMO Versus Small Cells," *IEEE Trans. Wireless Commun.*, vol. 16, no. 3, pp. 1834–1850, Mar. 2017.

[21] G. Interdonato, P. Frenger, and E. G. Larsson, "Scalability Aspects of Cell-Free Massive MIMO," in *ICC 2019 - 2019 IEEE International Conference on Communications (ICC)*, May 2019, pp. 1–6.

[22] C. Yang, Z. Chen, B. Xia, and J. Wang, "When ICN meets C-RAN for HetNets: an SDN Approach," *IEEE Commun. Mag.*, vol. 53, no. 11, pp. 118–125, November 2015.

[23] M. K. Karakayali, G. J. Foschini, and R. A. Valenzuela, "Network Coordination for Spectrally Efficient Communications in Cellular Systems," *IEEE Wireless Commun. Mag.*, vol. 13, no. 4, pp. 56–61, Aug 2006.

[24] R. Irmer *et al.*, "Coordinated Multipoint: Concepts, Performance, and Field Trial Results," *IEEE Commun. Mag.*, vol. 49, no. 2, pp. 102–111, February 2011.

[25] W. Choi and J. G. Andrews, "Downlink Performance and Capacity of Distributed Antenna Systems in a Multicell Environment," *IEEE Trans. Wireless Commun.*, vol. 6, no. 1, pp. 69–73, Jan 2007.

[26] X. Chen, X. Wang, and X. Chen, "Energy-Efficient Optimization for Wireless Information and Power Transfer in Large-scale MIMO Systems Employing Energy Beamforming," vol. 2, no. 6, pp. 667–670, Dec. 2013.

[27] G. Yang, C. Ho, R. Zhang, and Y. Guan, "Throughput Optimization for Massive MIMO Systems Powered by Wireless Energy Transfer," *IEEE J. Sel. Areas Commun.*, vol. 33, no. 8, pp. 1640–1650, Aug. 2015.

[28] L. Zhao, X. Wang, and K. Zheng, "Downlink Hybrid Information and Energy Transfer with Massive MIMO," *IEEE Trans. Wireless Commun.*, vol. 15, no. 2, pp. 1309–1322, Feb. 2016.

[29] D. Kudathanthirige, R. Shrestha, and G. A. Aruma Baduge, "Max-Min Fairness Optimal Rate-Energy Trade-Off of SWIPT for Massive MIMO Downlink," *IEEE Commun. Lett.*, vol. 23, no. 4, pp. 688–691, Apr. 2019.

[30] Y. Zhu, L. Wang, K. Wong, S. Jin, and Z. Zheng, "Wireless Power Transfer in Massive MIMO-Aided HetNets with User Association," *IEEE Trans. Commun.*, vol. 64, no. 10, pp. 4181–4195, Oct. 2016.

[31] D. Kudathanthirige, R. Shrestha, and G. A. Aruma Baduge, "Wireless Information and Power Transfer in Relay-Assisted Downlink Massive MIMO," *IEEE Trans. on Green Commun. and Netw.*, vol. 3, no. 3, pp. 789–805, Sep. 2019.

[32] R. Shrestha and G. Amarasuriya, "SWIPT in Hybrid Relay-Assisted Massive MIMO Downlink," in *Proc. IEEE Int. Conf. Commun. (ICC)*, May 2019, pp. 1–7.

[33] F. Yuan *et al.*, "Joint Wireless Information and Energy Transfer in Massive Distributed Antenna Systems," *IEEE Commun. Mag.*, vol. 53, no. 6, pp. 109–116, Jun. 2015.

[34] T. L. Marzetta, E. G. Larsson, H. Yang, and H. Q. Ngo, *Fundamentals of Massive MIMO*. Cambridge University Press, Cambridge, UK, 2016.

[35] S. Atapattu and J. Evans, "Optimal Energy Harvesting Protocols for Wireless Relay Networks," *IEEE Trans. Wireless Commun.*, vol. 15, no. 8, pp. 5789–5803, Aug 2016.

[36] G. Interdonato, H. Q. Ngo, E. G. Larsson, and P. Frenger, "How Much Do Downlink Pilots Improve Cell-Free Massive MIMO?" in *Proc. IEEE Global Communications Conference (GLOBECOM)*, Dec 2016, pp. 1–7.

[37] S. M. Kay, *Fundamentals of Statistical Signal Processing: Estimation Theory*. Englewood Cliffs, NJ: Prentice Hall, 1993.

[38] H. Q. Ngo and E. G. Larsson, "No Downlink Pilots are Needed in TDD Massive MIMO," *IEEE Trans. Wireless Commun.*, vol. 16, no. 5, pp. 2921–2935, May 2017.

[39] P. Marbach, "Priority Service and Max-Min Fairness," *IEEE/ACM Trans. Netw.*, vol. 11, no. 5, pp. 733–746, Oct 2003.

[40] B. Radunovic and J. Le Boudec, "A Unified Framework for Max-Min and Min-Max Fairness with Applications," *IEEE/ACM Trans. Netw.*, vol. 15, no. 5, pp. 1073–1083, Oct 2007.

[41] L. Zheng, D. W. H. Cai, and C. W. Tan, "Max-min Fairness Rate Control in Wireless Networks: Optimality and Algorithms by Perron-Frobenius Theory," *IEEE Trans. Mobile Comput.*, vol. 17, no. 1, pp. 127–140, Jan 2018.

[42] E. Bjornson, E. A. Jorswieck, M. Debbah, and B. Ottersten, "Multiobjective Signal Processing Optimization: The way to balance conflicting metrics in 5G systems," *IEEE Signal Process. Mag.*, vol. 31, no. 6, pp. 14–23, Nov. 2014.

[43] A. L. Peressini, F. E. Sullivan, and J. J.J. Uhl, *The Mathematics of Nonlinear Programming*. Springer-Verlag, 1988.

[44] S. Boyd and L. Vandenberghe, *Convex Optimization*. Cambridge University Press, 2004.

[45] M. S. Lobo, L. Vandenberghe, S. Boyd, and H. Lebret, "Applications of Second-Order Cone Programming," *Linear Algebra and its Applications*, vol. 284, no. 1, pp. 193 – 228, Nov 1998.

[46] M. Medard, "The Effect Upon Channel Capacity in Wireless Communications of Perfect and Imperfect Knowledge of the Channel," *IEEE Trans. Inf. Theory*, vol. 46, no. 3, pp. 933–946, May 2000.

[47] H. Cramer, *Random Variables and Probability Distributions*. Cambridge University Press, 1970.



Diluka Loku Galappaththige (S'18) received the B. Sc. degree (with first class Hons.) from the Department of Electrical and Electronic Engineering, University of Peradeniya, Sri Lanka, in 2017. He is currently working towards the Ph.D. degree in the Department of Electrical and Computer Engineering, Southern Illinois University, Carbondale, IL, USA. His current research interests include cell-free massive MIMO systems and intelligent reflective surfaces.



Rajan Shrestha received the B.E. degree in electronics and communications engineering from Tribhuvan University, Nepal, in 2014 and the M.Sc. degree from the Department of Electrical and Computer Engineering, Southern Illinois University, Carbondale, IL, USA, in 2018. He is currently an RF Analyst with Global Wireless Solutions, Inc., Dulles, VA, USA. His current research interests include wireless energy harvesting.



Gayan Amarasuriya Aruma Baduge (S'09, M'13, SM'19) received the B.Sc. degree in Engineering (with first class Hons.) from the Department of Electronics and Telecommunications Engineering, University of Moratuwa, Moratuwa, Sri Lanka, in 2006, and the Ph.D. degree in Electrical Engineering from the Department of Electrical and Computer Engineering, University of Alberta, Edmonton, AB, Canada, in 2013. He was a Postdoctoral Research Fellow with the Department of Electrical Engineering, Princeton University, Princeton, NJ, USA from 2014 to 2016. Currently, he is an assistant professor in the Department of Electrical and Computer Engineering in Southern Illinois University, IL, USA. He is an Associate Editor for IEEE Communications Letters, IEEE Wireless Communications and IEEE Open Journal of the Communications Society.